Master Thesis in Geographical Information Science nr 159

Use of Satellite Remote Sensing for Detecting Archaeological Features: An Example from Ancient Corinth, Greece

Manolis Papadakis

2023

Department of

Physical Geography and Ecosystem Science

Centre for Geographical Information Systems

Lund University
Sölvegatan 12

Manolis Papadakis (2023). Use of Satellite Remote Sensing for Detecting Archaeological Features: An Example from Ancient Corinth, Greece
Master degree thesis, 30/ credits in Master in Geographical Information Science
Department of Physical Geography and Ecosystem Science, Lund University

Abstract

During the last few decades, satellite remote sensing has proven to be an important non-invasive method for archaeological research in order to detect ancient sites and manage exposed architectural remains. Furthermore, multi-spectral satellite images, by offering bands that cover a wide range in the electromagnetic spectrum, can also help archaeologists to identify potential sub-surface remains, at depths from few centimeters to up a meter. However, their implementation usually takes place in a rural setting while there are often difficulties in validating the results. The site of Ancient Corinth and its rich archaeological record gives us the opportunity to apply some established image processing techniques, like vegetation indices and classification, in a semi-rural environment and compare them with known excavated features. This can help us test and evaluate the application of established image processing techniques for this purpose and potentially add more information to the archaeological background of the region.

Keywords: GIS, satellite remote sensing, vegetation indices, classification, archaeology

Acknowledgements

First and foremost, I am deeply indebted to my supervisor, Dr. Torbern Tagesson, for his continuous support and guidance. His advice carried me through all the stages of this dissertation and his high standards helped significantly in advancing this current work but also in causing me to think of research problems in ways I have not done before.

I am also grateful to the American School of Classical Studies at Athens – Corinth Excavations for supporting this work and especially to architect James Herbst for providing me with the necessary data and material to complete this thesis. I would like to extend my sincere thanks to Dr. Apostolos Sarris, Professor of Digital Humanities at the University of Cyprus, for all the fruitful conversations we had all these years and for providing me with the Geoeye images, without which this would have been a very different project. Thanks should also go to Dr. Guy D. R. Sanders, Director Emeritus of Corinth Excavations, for giving me permission to use the data from his 2001 geophysical survey.

Finally, I would like to thank my family for their continuous support and above all my partner Nina. Her emotional support and being there for me to all my ups and downs has kept me motivated and focused until the end.

Contents

List of figures and tables

List of vegetation indices equations

1. *DVI*: PNIR – PRED
2. *NDVI*: (PNIR – PRED) / (PNIR + PRED)
3. *EVI*: 2.5 * ((PNIR – PRED) / ((PNIR) + (C1 * PRED) – (C2 * PBLUE) + L))
4. *ARVI*: (PNIR – (2 [PRED – PBLUE])) / (PNIR + (2 [PRED – PBLUE]))
5. *SAVI*: ((PNIR – PRED) / (PNIR + PRED + L)) * (1 + L)
6. *MSAVI*: ((PNIR – PRED) / (PNIR + PRED - L)) * (1 + L)
7. *SR*: PNIR / PRED
8. *SQRT SR*: SQRT (PNIR / PRED)
9. *MSR*: (PNIR/PRED – 1)/((PNIR/PRED)1/2 + 1

Abbreviations

ARVI: Atmospherically Resistant Vegetation Index

ASCSA: American School of Classical Studies at Athens

CRS: Coordinate Reference System

DVI: Difference Vegetation Index

EVI: Enhanced Vegetation Index

GIS: Geographic Information System

GS: Gram-Schmidt

GSD: Ground Sampling Distance

IHS: Intensity-Hue-Saturation

IR: Infrared

ISODATA: Iterative Self-Organizing Data Analysis Technique

MLC: Maximum Likelihood Classification

MSAVI: Modified Soil-Adjusted Vegetation Index

MSR: Modified Soil Ratio

NDVI: Normalized Difference Vegetation Index

NIR: Near Infrared

PAN: Panchromatic

PCA: Principal Component Analysis

RS: Remote Sensing

SAVI: Soil-Adjusted Vegetation Index

SQRT SR: Square-Root Simple Ratio

SR: Simple Ratio

UV: Ultraviolet

VHS: Very High Resolution

VIS: Visible

1. INTRODUCTION

Archaeology is the discipline that helps us understand past cultures through the study of the physical remains of the human past, ranging from small objects to large buildings (Gamble, 2004). The main approach for collecting data in archaeological research is through excavation, a process that has been largely considered as intrusive and unrepeatable but also as the only source of actual evidence (Barker, 1993; Champion, 1980). During this process, large quantities of soil are removed while unearthed data (objects, structures, strata) can only be properly recorded once. Even though excavation still is the primary investigation tool, archaeologists have tried in the recent past to embed other methods and tools in their research, such as Geographic Information Systems (GIS), image processing techniques and geophysical methods, as non-destructive approaches that can allow a wider perception of archaeological landscapes, predict past behaviors as well as limit the need for excavations (Chapman, 2006).

During the last few decades, satellite remote sensing has been increasingly used in archaeology as a major, non-invasive method for not only detecting but also managing archaeological sites (Agapiou & Lysandrou, 2015). Adding to traditional means of visually identifying archaeological features from satellite and aerial imagery, like the detection of soil and crop marks, multi-spectral satellite images offer bands that cover a wide range of the electromagnetic spectrum and can help archaeologists identify potential sites at depths of few centimeters to up a meter (Lasaponara & Masini, 2011). Through the application of vegetation indices, archaeologists are using differentiations in spectral signatures, usually described as “anomalies” (Grøn et al., 2011), in order to find if there are any man-made structures beneath soil and vegetation that cannot otherwise be seen with the naked eye (Luo et al., 2019; Pan et al., 2017). Furthermore, classification techniques have been employed, to a lesser extent, for the study of above ground features. Supervised and unsupervised classifications have been used for the mapping and monitoring of exposed archaeological remains and excavation areas (Agapiou, 2020; Lasaponara & Masini, 2012b; Laet et al., 2009) and less for the detection of buried features (Ciminale et al., 2009). In Greece, satellite images and the application of the above methods have helped before to detect exposed and sub-surface remains (Rowland & Sarris 2007)), to analyze ancient urban development (Donati & Sarris 2016) and to manage archaeological sites (Liu et al 2003). However, all the

aforementioned methods seem to have two characteristics in common. Firstly, their implementation, usually, takes place in a rural setting and secondly there are often difficulties in validating the results.

The modern village of Ancient Corinth, in southern Greece, has been almost continuously inhabited since antiquity and is a product of constant development and changes in the surrounding landscape. At the same time, it has captured the attention of archaeologists from early on, resulting in an archaeological record that has been continuously expanding for more than a century. However, until today, no analysis of multispectral satellite imagery has been conducted in this region in order to identify or map either buried or exposed archaeological features. Furthermore, any aerial reconnaissance of possible features that has been conducted in the past, for the study of the ancient urban planning, has been based solely on the visual examination of satellite and aerial imagery, and no further image processing (Romano & Shoenbrun, 1993). As a result, this thesis aims at bridging this gap in the digital survey of the area and try to detect both visible and invisible parts of the ancient city. There will be an examination of the effectiveness of different satellite remote sensing techniques in the archaeological survey of this semi-rural region, including the detection of buried features through vegetation indices and unsupervised classification as well as the mapping of existing remains through different classification methods. It is anticipated that through this study we will not only be able to confirm the results of previous research but will also investigate new areas and possibly add new information about the archaeological background of the region. The archaeological record of Corinth gives us the opportunity to apply the aforementioned techniques and compare them with known features that have been excavated and investigated in the last decades. This can potentially help us understand better how these techniques work and possibly the extent to which they can be trusted.

Consequently, the overall aim of this thesis is to use satellite imagery as an archaeological tool for the detection and mapping of buried and exposed archaeological features while at the same time to test and evaluate the application of established image processing techniques for this purpose, in a semi-rural environment.

The main research questions of this thesis are:

- How can multispectral imagery contribute to the identification of past human-made structures in a semi-rural environment?
- How can different processing techniques and classification methods be used in an archaeological research context?

More specifically:

- Which vegetation indices seem to be more useful in the investigation of buried archaeological features?
- How may unsupervised classification be useful for the investigation of buried archaeological features?
- Are unsupervised or supervised classification techniques more useful when mapping exposed archaeological remains?

2. THEORETICAL BACKGROUND

2.1 Basic Principles in Remote Sensing

In a broader sense, remote sensing (RS) is the science of obtaining information about an object, area or a phenomenon by analyzing data that was acquired through a sensor and without coming into direct contact with the object under investigation (Lillesand et al., 2015). This can include the use of sensors, radars, lasers or scanners mounted on devices and measuring different physical aspects of an object or area (measuring the magnetic field, electric resistivity, electromagnetic energy etc.). Aerial photography or geophysics can be also be considered as a form of remote sensing. Usually, the data acquired from these sensors, is translated to images, which can afterwards be processed and analyzed.

Some scholars give a more specific definition of remote sensing, as the measuring, analysis and interpretation of electromagnetic radiation that is reflected or emitted from the Earth's surface and the atmosphere (Campbell & Wynne, 2011). This is related to Earth observation and is achieved via the use of satellite- or air-borne sensors (Mather & Koch, 1999). Today, this is the most common definition when we discuss remote sensing and this method is the one associated with this thesis.

The main principle behind remote sensing is that different objects on the Earth's surface reflect electromagnetic energy at varying wavelengths of the electromagnetic spectrum, thus creating a distinctive spectral signature. Consequently, these differences may allow us to identify different objects.

The complete range of electromagnetic waves with different wavelengths constitutes the electromagnetic spectrum (ITC, 2001). This spectrum extends from below 1nm wavelengths (gamma rays) up to several hundred meters (radio waves). As an example, the visible spectrum is approximately between 0.4-0.7μm, the near infrared (NIR) can be found at 0.7-1.2μm and the ultraviolet at 0.01-0.4μm. Two different materials may have similar spectral signatures in one wavelength and differ greatly in other areas of the spectrum (Lillesand et al., 2015). All objects or material on Earth's surface reflect or emit energy differently at different wavelengths, thus defining its characteristic spectral signature. Radiance is a measurable unit, expressed in W/m^2 and it is the variable that is measured by remote sensing sensors. Reflectance is a property,

described as the ratio of the reflected radiance from the target to the incoming radiance reaching the target (Lillesand et al., 2015). As an example, healthy vegetation has high reflectance in the near IR part of the spectrum while water reflects mostly in the blue wavelengths (0.4-0.5μm) (ITC, 2001). Healthy leaves strongly reflect energy in the near infrared and more moderately in the green portion of the spectrum but since green is in the visible spectrum, we see vegetation as green (Limp, 1993). However, even in the same material class, the spectral reflectance may still vary considerably (Campbell & Wynne, 2011) (Figure 1).

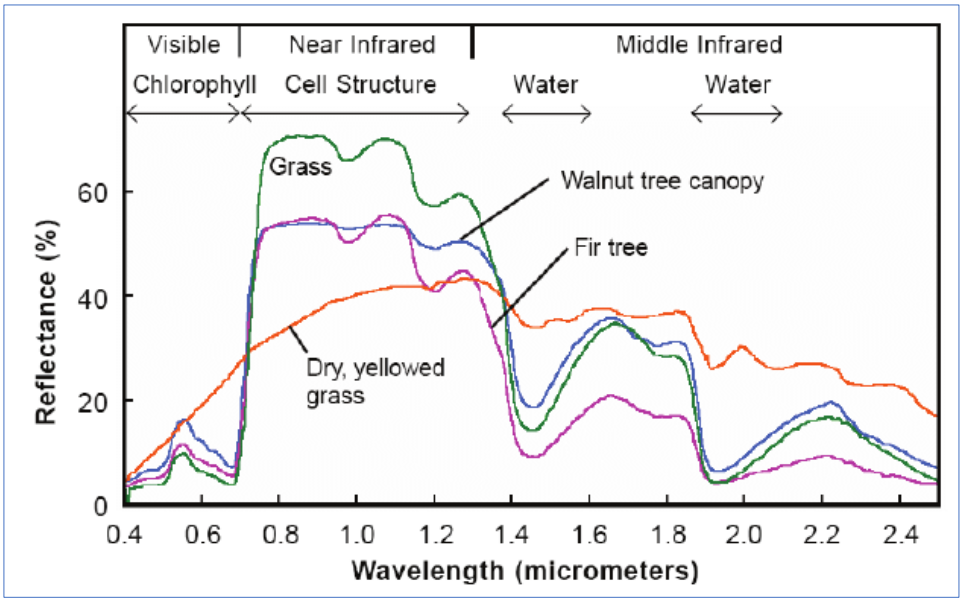

Figure 1: Reflectance of different types of green vegetation (Smith, 2001).

2.2 Sensors and Image Processing

The measurement of radiance by sensors can be conducted either passively or actively. Passive sensors depend on the reflected solar radiation or the emitted terrestrial radiation (e.g., multispectral scanner, thermal scanner) while active sensors generate their own source of electromagnetic radiation (e.g., laser scanner) (Barnsley, 1999). Here, we are concerned with the former category of sensors and more specifically with those mounted on satellites, thus constituting what is called satellite or space-borne remote sensing.

The part of the electromagnetic spectrum that is most commonly used in remote sensing is between the ultraviolet (UV) and micro and radio waves (Lillesand et al., 2015), which can help researchers retrieve information otherwise not perceptible to the human

eye. In remote sensing imagery, several types of resolution are critical in order to assess the usefulness of an image for a specific purpose or project. Resolution is defined as "the ability of the system to render the information at the smallest discretely separable quantity in terms of distance (spatial), wavelength band of electromagnetic radiation (spectral), time (temporal) and/or radiation quantity (radiometric)" (Aggarwal 2004b).

Spatial resolution indicates the smallest unit area that can be measured (ITC 2001). It defines, in practical terms, how big a pixel is sized and how much detail you can get on ground level. The finer the spatial resolution is the higher the ability to recognize different features on the Earth's surface. Nowadays, sensors can be differentiated, based on spatial resolution, in low resolutions systems (approx. >1km, e.g., NOAA-AVHRR), medium resolution systems (approx. 100m – 1km, e.g., Terra-MODIS), high resolution systems (approx. 5 – 100m, e.g., Landsat TM/ETM+) and very-high resolution systems (approx. <5m, e.g., GeoEye, WorldView) (Liew, 2001).

Spectral resolution describes the range of the electromagnetic spectrum measured by a sensor (ITC 2001), meaning how many bands or channels a sensor has and how broad those are (Limp 1993). Based on the number of spectral bands, optical imaging systems can be further categorized to monospectral (a single wavelength band), multispectral (several broad spectral bands, normally ≥10nm wide) and hyperspectral (spectral bands, normally defined as ≤10nm wide) (Giardino & Haley, 2006; Liew, 2001).

Temporal resolution describes the ability of a sensor to take images of the same area and at the same viewing angle, at different moments in time (Aggarwal 2004b). For example, Landsat-7 has a temporal resolution (or return period) of 16 days and IKONOS 14 days. Finally, radiometric resolution measures the levels of energy that can be observed by a sensor (ITC 2001) and its ability to distinguish between values of an acquired image. The finer the radiometric resolution the better the sensor is to detect small differences in reflected energy.

Multispectral sensors store electromagnetic radiance measurements as digital number (DN) values (ITC 2001). In a multispectral image, each pixel includes multiple DN values, each one corresponding to a different spectral band. The characteristics of an image define the quality of a captured scene, as related to the different kinds of resolution described above. Furthermore, different methods and techniques can be employed to improve image quality for further analysis and interpretation. These

methods are applied on pixel level, using predefined equations and usually resulting in a new raster image that can be further manipulated. Band combinations are probably the most basic form of spectral enhancement and refers to the assignment of different colors in order to represent brightness in different regions of the spectrum (Campbell & Wynne, 2011).

2.3 Remote Sensing methods in archaeological research

Pan sharpening

Pan-sharpening or image fusion is a technique used to combine the high spatial resolution of a panchromatic band (a single-band grayscale image) with the spectral information of other multispectral bands, which usually have a lower spatial resolution. The result can be a composite multispectral image with very high spatial resolution, which can be very helpful in the investigation of sub-meter archaeological marks. For this to be achieved, usually, the set of multispectral and panchromatic images to be fused should not have discrete differences in ground cover, sun illumination or viewing angle. This means that most commonly they should be acquired by the same sensor even though there can be cases that images from different sensors can be combined (Agapiou, 2020). Over the years, a number of algorithms have been developed and evaluated for pan-sharpening, such as the Intensity-Hue-Saturation sharpening (HIS), Brovey transformation, Gram-Schmidt (GS) and Principal Component Analysis (PCA) (Sarp, 2014; Lasaponara & Masini, 2012c).

The Gram-Schmidt (GS) method is based on an orthogonalization process. Initially, a panchromatic simulation takes place by computing a weighted average of the multispectral bands. Next, a GS transformation is performed for the simulated higher-resolution band and the multispectral bands, where the panchromatic is employed as the first band. Finally, the panchromatic band is replaced with the first GS component and an inverse GS transform is applied to create the higher resolution multispectral image (Sarp, 2014; Laben & Brower, 2000).

Vegetation Indices

Vegetation indices are well-established in archaeological research and have been widely used for the observation of changes in vegetation growth and the possible existence of underlying archaeological features (Kalayci et al., 2019; Donati & Sarris,

2016; Agapiou et al., 2014; Sarris et al., 2013; Lasaponara & Masini, 2012a). By using equations that combine two or more bands, we can differentiate green vegetation as compared to brown and other materials. Even though most of the indices used are closely correlated, usually they are all included as different indices are more sensitive in different ranges of biomass and groundcover (Prabhakara & Hively, 2015). The most common indices used in archaeology are the following:

DVI (Difference Vegetation Index)

This index follows a simple equation for distinguishing vegetation and soil (Naji, 2018). However, it is sensitive to the amount of vegetation and it cannot handle differences between reflectance and radiance caused by atmospheric effects.

1. $$DVI = P_{NIR} - P_{RED}$$

NDVI (Normalized Difference Vegetation Index)

This is the most typical vegetation index, useful for distinguishing vegetation from soil and indicating the amount of vegetation (Tucker, 1979). When executed, resulting values range from -1 (unhealthy/no vegetation) to 1 (healthy). Through NDVI, we can monitor the greenness in plants. However, it can be sensitive to atmospheric effects and soil brightness, and saturates at high biomass levels (Mutanga & Skidmore, 2004):

2. $$NDVI = (P_{NIR} - P_{RED}) / (P_{NIR} + P_{RED})$$

EVI (Enhanced Vegetation Index)

The EVI index was conceived to avoid the issue of saturation of the NDVI at high biomass loads and was originally developed for MODIS data (Matsushita et al., 2007). Hence, it can be useful for areas with dense vegetation and high amount of chlorophyll. In EVI, coefficients C1 and C2 have been added, for the correction of aerosol scattering in the atmosphere, and L to adjust soil noises. Usually, this corresponds to C1=6, C2=7.5 and L=1. Resulting values should range between -1 to 1.

$$EVI = 2.5 * ((P_{NIR} - P_{RED}) / ((P_{NIR}) + (C1 * P_{RED}) - (C2 * P_{BLUE}) + L))$$

ARVI (Atmospherically Resistant Vegetation Index)

The ARVI index can be relatively insensitive to atmospheric effects and it can be useful for regions with high atmospheric aerosol concentrations, high amount of rain, fog or air pollution (Kaufman & Tanre, 1992). It follows the structure of the NDVI index with the addition of the blue wavelength in the equation:

4. $$ARVI = (P_{NIR} – (2\ [P_{RED} – P_{BLUE}])) / (P_{NIR} + (2\ [P_{RED} – P_{BLUE}]))$$

SAVI (Soil Adjusted Vegetation Index)

The SAVI index is useful for mitigating the impact of soil brightness (Huete, 1988). It is based on NDVI, with the addition of a soil adjustment factor L in order to correct soil noises (like soil moisture and color). Resulted values can range from -1 to 1. The L factor equals 0 for areas with high green vegetation and 1 for those with low vegetation.

5. $$SAVI = ((P_{NIR} – P_{RED}) / (P_{NIR} + P_{RED} + L)) * (1 + L)$$

MSAVI (Modified Adjusted Vegetation Index)

The MSAVI index follows the SAVI index, using the L factor. It can be useful in areas with low vegetation, minimizing the effect of bare soil.

6. $$SAVI = ((P_{NIR} – P_{RED}) / (P_{NIR} + P_{RED} - L)) * (1 + L)$$

SR (Simple Ratio)

Also known as Ratio Vegetation Index (RVI), it appears with high reflection for vegetation and low for soil and other materials, indicating the amount of vegetation (Jordan, 1969). As the amount of green vegetation increases in a pixel, the SR increases:

7. $$SR = P_{NIR} / P_{RED}$$

SQRT SR (Squared-root Simple Ratio)

This index follows the SR logic but it helps in decreasing the saturation issue at high biomass levels (Mutanga & Skidmore, 2004).

8. $$SQRT\ SR = SQRT\ (P_{NIR} / P_{RED})$$

MSR (Modified Simple Ratio)

The Modified Simple Ratio is a modification of SR and NDVI and it is considered to be more sensitive to biophysical parameters of vegetation (Chen, 1996).

9. $$MSR = (P_{NIR}/P_{RED} - 1)/((P_{NIR}/P_{RED})^{1/2} + 1$$

Land cover classification

The overall objective through classification is to, automatically or semi-automatically, categorize all pixels into land cover classes or themes. This can take place through a spectral pattern (pixel spectral information) or a spatial pattern recognition (pixel spatial relationship) (Lillesand, 2015).

Through supervised classification, a stronger user interaction is expected and a relevant knowledge of the study area and the possible classes under investigation is required. The two basic steps are a) the training session, in which we identify representative areas that share similar spectral characteristics and may belong to the same land cover type and b) the classification stage, in which the image pixels are categorized into classes, by comparing their spectral signatures. When creating the training samples, the intention is to "teach" the computer to recognize pixels of same value. The spectral signatures of these samples are used to classify the image (Lillesand, 2015).

In unsupervised classification, the process is fully automated and all pixels are categorized in a pre-defined number of classes, based on their reflectance values (Lillesand, 2015). User interaction is more limited, compared with the supervised method, and a prior knowledge of the area and of potential classes is not really required, since the identity of spectral classes is not really known. Based on the pixel values of the available bands, the computer is trying to statistically generate clusters and create groups of land cover classes.

Accuracy assessment constitutes an integral part of land cover classification, in order to determine how accurate, the information depicted in the derived maps is. During this process, data from the remote sensing-based classes is compared with data corresponding to the actual land cover. This validation data is usually gathered in the field, through different sampling methods, such as random or systematic sampling and is often called "ground-truth" data. However, it is not uncommon that this data can be collected through the use of satellite imagery; this is more often the case when

inaccessible landscapes are involved (Kumar, 2019; Ramzi, 2015). After the validation and map data are co-registered, they are compared on a class-by-class basis, by creating an "error" or "confusion matrix", which results into measuring different accuracy levels, like overall, "producer" or "user" accuracy (Lillesand et al. 2015; Campbell & Wynne, 2011). A further statistic that is usually calculated following the accuracy assessment is the *kappa* (κ) coefficient. This indicates the extent to which the percentage correct values of an error matrix are due to "true" agreement versus "chance" agreement. *Kappa* ranges from -1, meaning the mapped classes do not correspond to validation data at all, to 1, meaning there is absolute agreement. A *kappa* of 0 suggests that a given classification is no better than a random assignment of pixels (Lillesand et al., 2015).

2.4 Remote Sensing in Archaeology and Cultural Resources Management

Compared to other remote sensing and image analysis techniques (geophysics, aerial imagery, GIS analysis), satellite remote sensing offers the extra advantage to archaeologists of being able to see an entire landscape at different resolutions and scales as well as covering unreachable areas or areas of great extent (Parcak, 2009). Through remote sensing, researchers can detect new sites and observe features that would otherwise be difficult to see at ground level as well as establish spatial relationships and connections with neighboring sites and areas of archaeological interest (Giardino & Haley, 2006; Agapiou et al., 2013; Lasaponara & Mansini, 2007). At the same time, satellite images constitute a major non-invasive method not only for mapping but also for managing archaeological sites, monitoring changes through long periods of time and preventing destruction from urbanization, looting and environmental changes (Parcak et al., 2017; Agapiou et al., 2015; Hadjimitsis et al., 2013; Parcak, 2007).

The use of remote sensing in archaeology for the detection of sites of archeological interest started as early as in the 1920s, after WWI, with the use of aerial photography. The first satellite images to be used by archaeologists were those taken by the CORONA spy satellites (Casana, 2020). After their declassification, US (CORONA – Key Hole program) and former Soviet Union (KV-1000) spy satellite photography were used due to their high spatial resolution, of up to 2m and their broad time span (1959-1972); thus, allowing the monitoring of gradual changes in land use and land cover over the past century (Luo et al., 2019).

The earliest multispectral satellite system that was used for archaeological research was Landsat, providing long time series of multispectral data, at moderate to high spatial resolution (Luo et al., 2019; Dorsett et al., 1984), followed by SPOT in the 1980's. Since 1972, Landsat has been used in various projects across Europe (Hadjimitsis et al., 2013). In 1999, the launch of IKONOS, the first commercial, very high-resolution satellite, was a major improvement for archaeological research applications, rendering remote sensing technologies as pivotal in archaeological research and initiating a significant rise in related studies (Agapiou & Lysandrou, 2015).

Today a wide range of high and very high-resolution (VHR) images is used from different satellites, such as IKONOS, SPOT, Quickbird, WorldView and GeoEye. These commercial satellites even though they may be lacking in the range of spectral information compared to Landsat (for example) are preferred due to the higher spatial resolution they can offer (Gennaro et al. 2019; Zanni & De Rosa, 2019; Donati & Sarris, 2016; Morehart & Millhauser, 2016; Ross et al. 2009; Garrison et al. 2008) (Table 1).

Even though very-high spatial resolution multispectral imagery has been considered as the most appropriate for detecting submeter land cover changes, open access and high-resolution imagery, like Google Earth applications, Landsat and Sentinel-2, either combined with each other or standalone, has also been proved useful for archaeological survey and heritage management (Luo et al., 2018, Agapiou et al., 2014).

Satellite	**Launch Date**	**Channels**	**Spatial Resolution**
SPOT 6/7	2012/2014	5 (PAN, VIS, NIR)	1.5m (PAN)
Ikonos 2	1999	5 (PAN, VIS, NIR)	1.0m (PAN)
Quickbird 2	2001	5 (PAN, VIS, NIR)	0.61m (PAN)
Worldview 2	2009	9 (PAN, VIS, NIR)	0.46m (PAN)
Geoeye 1	2008	5 (PAN, VIS, NIR)	0.41m (PAN)
Worldview 3	2014	29 (PAN, VIS, NIR, MIR)	0.31m (PAN)
Worldview 4	2016	5 (PAN, VIS, NIR)	0.31m (PAN)

Table 2: Selected satellites ordered by spatial resolution (after Lambers, 2018).

Traditional ways for visually identifying archaeological features from remote sensing imagery include the detection of variations in shadowing, soil color, crop marks, moisture patterning and thermal differences (Lasaponara & Masini, 2011; Giardino & Haley, 2006). Multi-spectral satellite images, by offering bands that cover a wide range of the electromagnetic spectrum (beyond visible bands and to the thermal infrared and radio microwaves), can further help archaeologists in this respect. Buried

archaeological remains are expected to alter the chemical, physical and biological properties of the soil, which in turn can be expressed by the phenological differences in the spectral reflectance of vegetation (Luo et al., 2019). Additionally, buried structures may produce an inhomogeneous distribution of humidity in the soil, which in turn can affect parameters, such as the density of the vegetation as well as the color and thermal properties of the soil (Orlando & Villa, 2011).

The detection of buried archaeological remains is usually performed by the application of different vegetation indices, such as the NDVI, in an effort to enhance possible crop marks while NIR to IR (Agapiou et al., 2012) and False Color Composites (FCC) have also been employed for the discovery of archaeological marks (Alexakis et al., 2009). The application of these indices is mostly based on visual interpretation and association with other known features and data in order to determine whether they could indicate buried archaeological remains while the validation of results is usually absent (Gennaro et al., 2019; Pan et al., 2017; Donati & Sarris, 2016). As it happens with other earth observation and cartography related disciplines, the processing of remotely sensed data in archaeology follows a somewhat standard procedure, encompassing image correction, radiometric and spectral enhancements, transformation and registration while analysis often entails classification methods, which can further assist to feature interpretation (Lambers, 2018; Lasaponara & Masini, 2012a).

Classification techniques, have been mainly used for the monitoring of known and above ground archaeological remains and a bit less for the detection of unknown features (Lasaponara & Masini, 2012b). Supervised pixel classification has been used to classify land cover of archaeological interest (Siart et al., 2008) and a combination of unsupervised and object-based classification in order to classify known remains and excavated areas (Laet et al., 2009). Unsupervised pixel classification has been applied for the detection of buried features through the spectral differences apparent in crop- and soil marks but with validation of results being again a limitation (Ciminale et al., 2009).

3. STUDY AREA AND PREVIOUS RESEARCH

The ancient city of Corinth was located where the modern village of Ancient Corinth stands today, about 80km southwest of Athens and at a distance of approximately 3km from the Corinthian Gulf, at a mean elevation of 76m above sea level. Corinth has always been a center for commercial activity, from early antiquity through medieval times. Its place on the north coast of the Peloponnesus peninsula, at a point that allowed the control of maritime routes from east to west and the main land traffic from mainland Greece toward south, rendered Corinth a center of communications and travels (Figure 2).

Figure 2: Greece and location of Corinth.

The local geology of Corinth consists mostly of marine sediments, marl clay, overlaid by layers of porous sandy or pebbly limestone (Sanders et al., 2018). The region has a complex geological history, comprising of several uplifts and changes in relative sea level, which have occurred during the last 300 000 years. This activity has resulted in the creation of a series of prominent flat terraces that run approximately parallel to the

coast of the Corinthian Gulf. They present steplike topographic features and scarps of various heights at their northern edges. (Hayworth, 2003). The core of the ancient city seems to have been extended on two of those terraces, one at approximately 90m and the other at about 60m above sea level. To the south of the city, the massive limestone rock of Acrocorinth rises at a maximum elevation of 579m above sea level.

There are traces of constant occupation in Corinth since the Neolithic times, ca. 6500 B.C. However, the city reached its acme from mid-8th to late 6th century B.C. During that time, temples and roadways were built while the city was enclosed with a ca. 10km long wall, having the top of Acrocorinth as its citadel. In the next years, from 5th to 2nd century B.C., a more thorough urban planning of the city was developed (Sanders et al., 2018). The Greek city was sacked by the Romans in 146 B.C. and Julius Caesar re-founded Corinth as a new colony, in 44 B.C., under the name of *Colonia Laus Ioulia Corinthiensis*, establishing a new urban plan. In the next five centuries, Corinth acquired organized public spaces, with a forum and public buildings, such as baths, temples and shops (Sanders et al., 2018; Romano, 1993). In the 6th century, the decreased population relocated into a smaller walled area (Late Roman wall), east of the Roman Forum (Gregory, 1979). Corinth survived in the medieval times as a small lively town, but ended up as a small village.

In 1858, after a major earthquake, the new city of Corinth was created a few kilometers to the north and the village of Ancient Corinth was inhabited by migrants from other nearby mountainous areas. During the 1950s and 1960s, the village's-built area expanded greatly and the cultivation of the area was intensified. Today, Ancient Corinth is a large sized village, having a population of ca. 3000 people. It is surrounded by fields, consisting mostly of olive groves and citrus fruits and secondarily of vineyards and other orchards. From the ancient Greek and Roman cities, the main areas that can be observed today are those of the forum, about the center of the village and the castle of Acrocorinth to the south.

Since 1896, the American School of Classical Studies at Athens (ASCSA) has been excavating at Corinth and they are responsible for the large volume of the recorded and published monuments of the region. The Greek Archaeological Service has also been conducting fieldwork and studying the area since the first decades of the 20th century. In 1987, the so called "Corinth Computer Project" was launched, having as its main

target the study of the city during the Roman period as well as the production of digital maps. During this project all excavated roads in the region were digitally recorded and incorporated with previous excavation state plans, while aerial photographs, coming from an early 1960s survey, conducted by the Hellenic Air Force, were used to identify "shadow lines" or crop marks, covering an area of more than 40km^2 (Romano & Tolba, 1995; Romano & Shoenbrun, 1993).

In the end, a suggested grid plan of the Roman city was produced, which followed the general rule of ancient urban planning, based on a grid-like system of roads with a central square (forum). The proposed plan covered an area of approximately 2265x1062m., with a primary roadway, the *cardo maximus*, running N-S and dividing the city in two nearly equal east-west segments and a major E-W road, the *decumanus maximus*, dividing the city in two also nearly equal north-south segments. Several other streets would run parallel to these N-S (*cardi*) and E-W (*decumani*) axes. This arrangement would have created buildings blocks (*insulae*) of varying lengths but of a steadier width of about 35.5m (1 roman actus) (Romano, 2003).

In 2001, an extended geophysical survey was conducted by the ASCSA, using electric resistivity. During this survey, large areas at the east and north of the village were covered, and the results, part of which will be used later, provided some further evidence for the potential course of the Late Roman wall.

In this project, research was limited in the region inside the ancient Greek circuit wall and the immediate outside environment, covering an approximate area of 6.5km^2 (Figure 3). This is a diverse area including the modern village of Ancient Corinth with the uncovered antiquities and archaeological sites, modern roads, cultivated fields and trees of different kinds. The features that are expected to be traced may belong to walls, which size usually varies between 0.50m and a couple of meters and streets, which originally could have a width of up to 3-4m but today would appear more reduced due to destructions and later alterations.

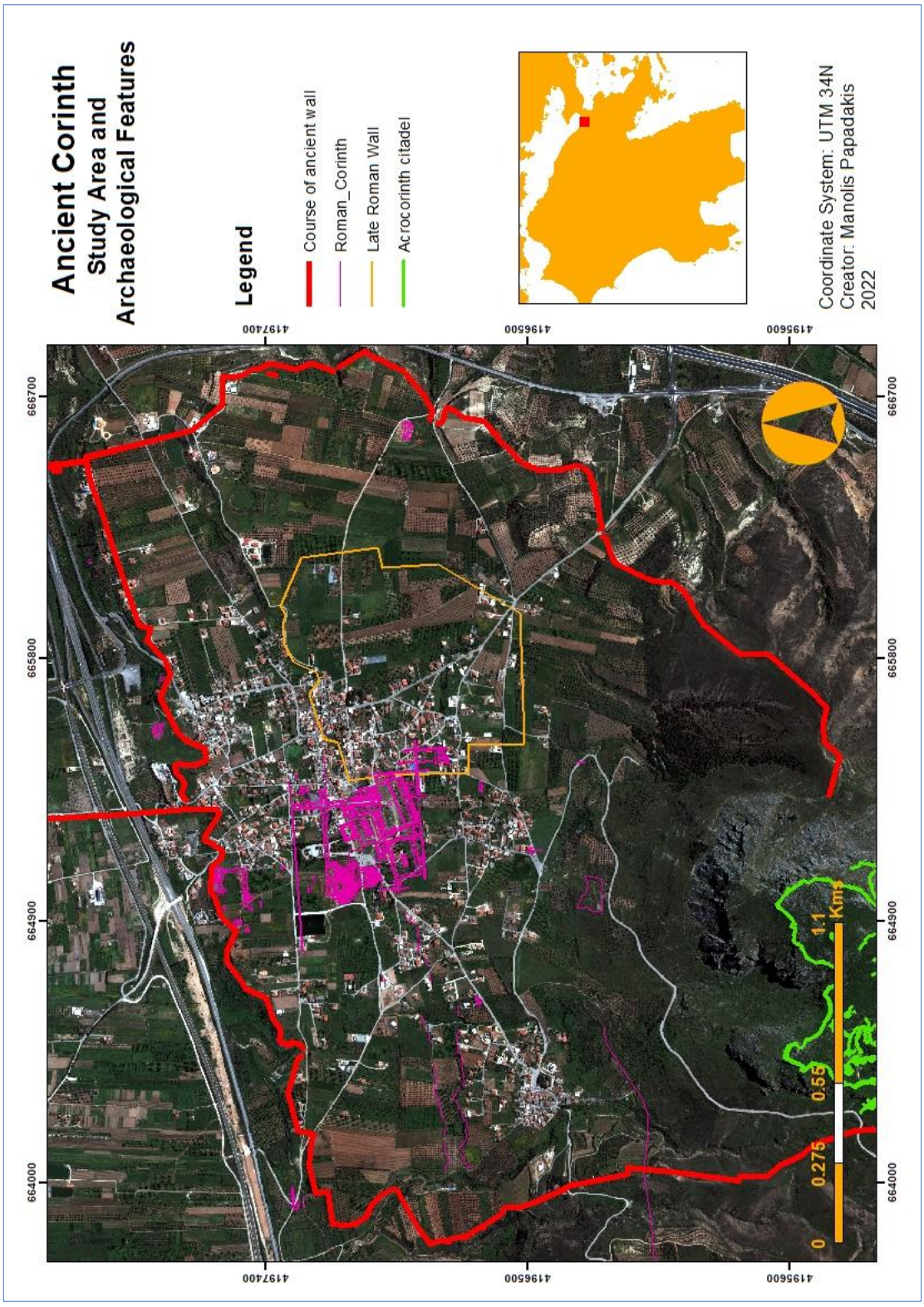

Figure 3: Study area.

4. MATERIALS AND METHODS

4.1 Data

Satellite data

In archaeological satellite remote sensing, VHR imagery seems to be the most appropriate as it proves to be more helpful in identifying subtle differences on the ground, compared with other, high to medium resolution imagery, such as that from Landsat or Sentinel. Since most of the features that we seek to find as anomalies in vegetation indices and map in classification can be from about 1-2m down to 0.50m wide, this project required data of very high spatial resolution. The spectral characteristics should cover the visible and infrared spectrum and have minimum cloud cover and a close-to-nadir angle in order to avoid shadows casted from other features, like modern buildings, as much as possible.

Two GeoEye-1 images, acquired on April 19, 2012, form the basis for the processing in this project. A panchromatic image, which comes at a resolution of 0.50m and a multispectral one (visible, NIR), which comes at a spatial resolution of 1.87m. GeoEye-1 was launched on September 2008, at an orbit height of 681km. The satellite follows a sun-synchronous orbit having a swath width of 15.2km with a revisit time at 1.7 days and descending node at 10.30am. The spectral bands of GeoEye-1 are limited to the visible and near infrared wavelengths (Hadjimitsis et al., 2013; https://earth.esa.int/eogateway/ missions/geoeye-1). The image was downloaded from DigitalGlobe.com and had already been geometrically and radiometrically corrected.

Archaeological features

Shapefiles of the uncovered archaeological features in the study area were used in order to compare and associate anomalies from the satellite imagery processing with known archaeological features (Figure 4). These shapefiles represent not only the visible remains but also their potential continuation in the landscape. The shapefiles were acquired by the American School of Classical Studies – Corinth Excavations and can also be viewed at ASCSA's webpage, at GIS section (ASCSA, 2022).

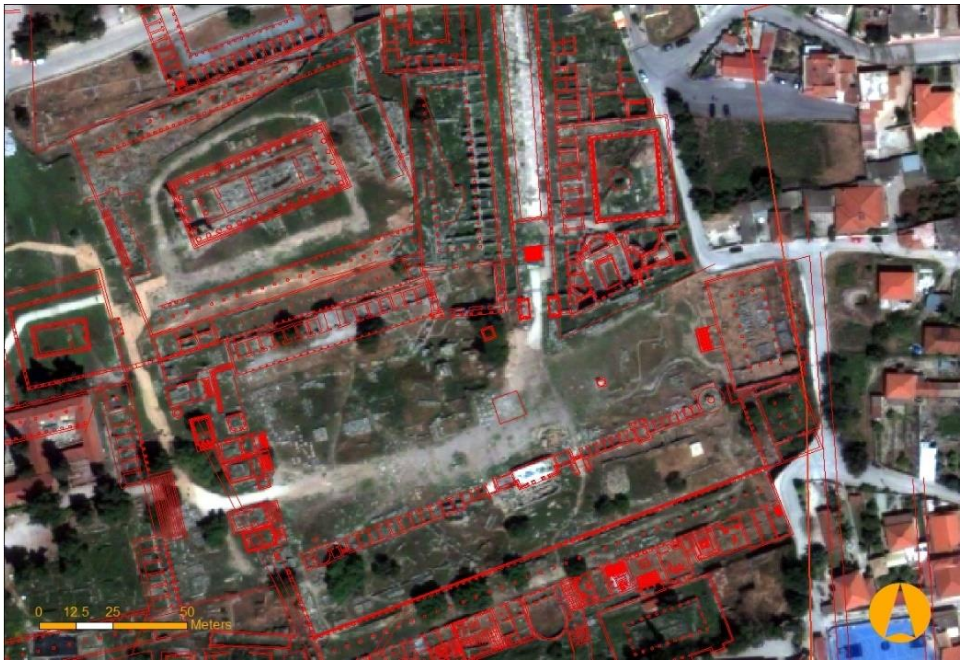

Figure 4: Detail of shapefile of known archaeological remains from the center of the archaeological site.

Validation data

Finally, further data sets were used at the accuracy assessment stage of this study. This included GPS points, which were taken in the field with a handheld Garmin Montana 650 device and where later extracted in a CSV file. A total of 63 points was collected along walls that were discovered in an area excavated in 2020 by the Greek Archaeological Service and which were used in this research in order to validate some vegetation indices anomalies that were observed in the 2012 Geoeye-1 image. For simplicity, we shall call this area here as "west of soccer field". In order to visualize these points and current state of the area, an image (screen dump) was downloaded by using Google Earth Pro, at 1m resolution, in JPEG format. This image was taken on June 6, 2021 (Figure 5).

Additionally, part of the geophysical data, from the 2001 survey, was used to validate anomalies that were observed during this study and which could be associated with part of the Late Roman wall. For that survey, electric resistivity was conducted, at 0.50 intervals sampling. This data was acquired as simple TIFF images, at a 0.20m spatial resolution.

Figure 5: Google Earth image with GPS points along the walls.

The Geoeye-1 image was delivered in the geographic coordinate system WGS84. The GPS points were collected in the same reference system. The shapefiles of the known archaeological features and excavated areas of the study area as well as the geophysics data follow a local grid system that has been created by ASCSA for the needs of the excavations. Lastly, the Google Earth image was missing spatial reference information (Table 2).

Data	Type	Details	Source
GeoEye-1	raster	**Panchromatic**: 0.50m resolution GSD. Spectral range: 0.45-0.9μm **Multispectral**: 1.87m resolution GSD. Spectral range: [blue] 0.45-0.51μm, [green] 0.52-0.58μm, [red] 0.65-0.69μm, [NIR] 0.78-0.92μm **Format**: GeoTIFF, 16-bit. **Angle:** 9.1^{o} off-nadir angle. **CRS**: WGS84. Extracted 19 April, 2012.	Digitalglobe.com / Provided by Prof. Apostolos Sarris (University of Cyprus)
"West of soccer field" GPS points	table	**Format**: CSV. **CRS**: WGS84. Collected 10 September, 2022.	Field survey
Google Earth image	raster	**CRS**: - **Format**: JPEG, 8-bit. Taken on June 6, 2021.	Google Earth Pro

Geophysics data	raster	**CRS**: Local Corinth Grid. **Format**: TIFF, 8-bit. Collected in 2001.	American School of Classical Studies – Corinth Excavations
Known archaeological features	vector	Data for walls, temples, excavation sites, graves etc. **Format**: ESRI shapefile **CRS**: Local Corinth Grid	American School of Classical Studies – Corinth Excavations

Table 2: Summary of data used in the study.

4.2 Methodology

The general methodology to identify and classify possible and visible archaeological features, consisted of the pre-processing and processing procedures, followed by the identification of anomalies, the validation of results and the production of land cover maps (Figure 6). All processing steps took place in ESRI's ArcGIS environment, using ArcMap 10.3 and the available tools for geoprocessing, spatial analysis and raster calculations.

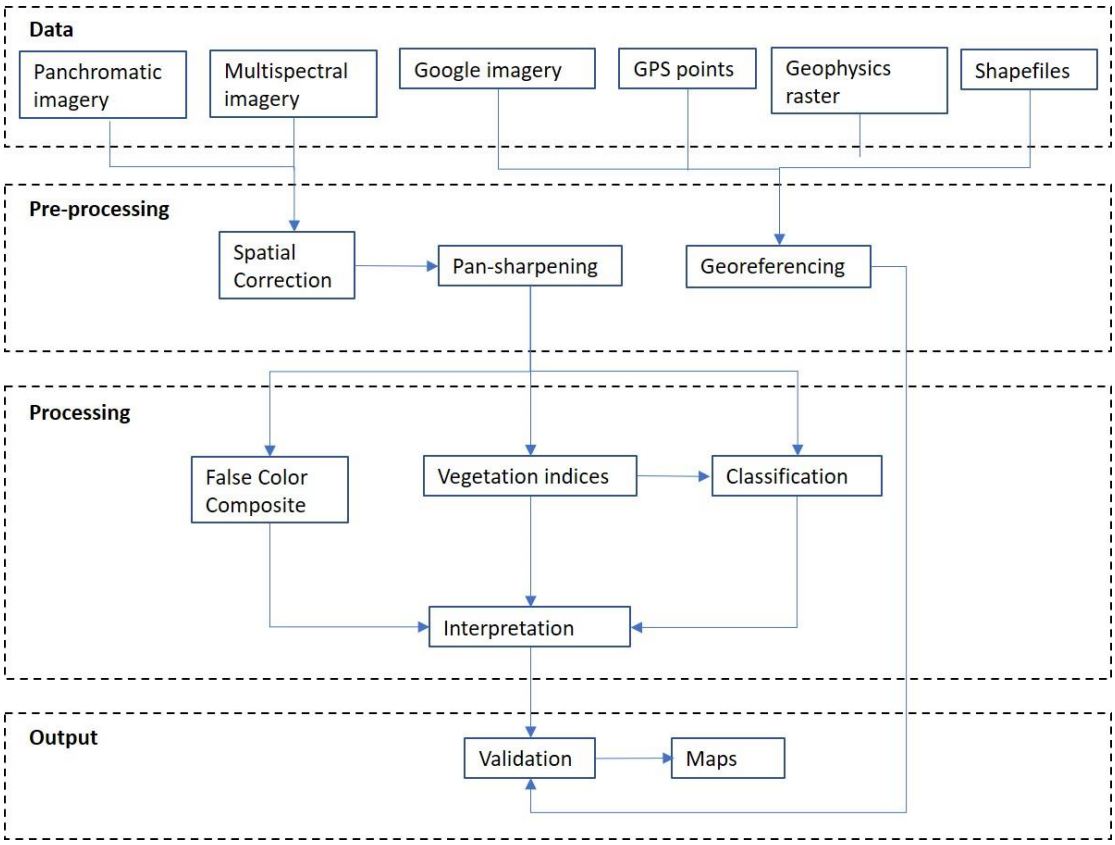

Figure 6: Methodology outline, showing the different processing stages.

4.2.1 Pre-processing

Pre-processing was focused mostly on the geometric correction and reprojection of raster and vector datasets as well as the pan-sharpening of the satellite panchromatic and multispectral images.

Georeferencing

As all datasets had a different origin, the first step was to reproject and georeference them in order to achieve an accurate overlap and measures. All data, rasters and shapefiles, were reprojected to the Universal Transverse Mercator (UTM) projected coordinate system zone 34N using a bilinear transformation method, and pixel values were resampled using *Nearest Neighbor*, as this option does not affect cell values. The CSV file of GPS points was imported as X, Y data and then saved as shapefile and reprojected in UTM 34N.

The Google Earth screen dump was georeferenced, using the reprojected GeoEye-1 image as reference. Known features in the landscape, such as the soccer field, buildings and roads were used as Ground Control Points. In total, 10 Ground Control Points were used, with a total Root Mean Square error of 0.97m. The image was then rectified and pixel values were resampled using the *Nearest Neighbor* option.

Pan-sharpening

Transformations were executed by using the available ArcGIS tool, *Create Pan-sharpened Raster*. The goal was to use the GeoEye panchromatic image in order to improve spatial resolution of the four GeoEye multispectral band images. The result is four multispectral images that retain their spectral information and acquire the spatial resolution of the panchromatic one, combined in a composite image. In this project, the Gram-Schmidt transformation was chosen as the preferred method in similar studies, when compared and evaluated with other pan-sharpening techniques (Agapiou, 2020; Sarp, 2014; Lasaponara & Masini 2012c). For the transformation, the weights suggested by ESRI for the GeoEye sensor were used (R, G, B, NIR: 0.6, 0.85, 0.75, 0.3). New images were exported as geoTIFFs. The Gram-Schmidt transformation did not show any significant distortions while the observation of known archaeological features was distinctive.

4.2.2 Processing procedures

Main processing consisted of the image enhancement techniques and the different classification methods. Image enhancement included the creation of a False Color Composite and the calculation of several vegetation indices and was focused on the investigation of possible buried archaeological features. The shapefiles of known archaeological features were examined along with the identified anomalies for further interpretation and cross-examination of results. Classification methods included supervised and unsupervised classification, in order to map exposed archaeological features and test their potential for further mapping/identifying possible buried remains and validating vegetation indices results.

Image enhancement

The first enhancement technique included the creation of a False Color Composite (FCC) in order to emphasize specific attributes of the pan-sharpened, multispectral image. A False Color Composite, which is commonly used for the evaluation of vegetation health and density, follows the combination NIR-R-G (4-3-2). With this combination, vegetation appears in different hues of red, water as black and soil and built areas in different hues of grey or tan/brown (Lillesand et al., 2015).

The second enhancement technique was to calculate the vegetation indices. More specifically, the following indices were calculated: NDVI, DVI, SAVI, MSAVI, SR, SQRT SR, MSR, ARVI and EVI (see theoretical background for further information). For estimating SAVI, L was set to 0.5 since the study area contains a mixture of vegetation and bare soil.

Classification

Both supervised and unsupervised classifications were employed so as to examine their potential for mapping visible archaeological features. Unsupervised classification was further used for detecting anomalies in vegetation that could indicate buried features. For the buried features, it was decided to only use unsupervised classification as a further automated method since the spectral characteristics of these archaeological features cannot be known a priori as we did not have enough reliable training samples.

Supervised classification for excavated features

For the supervised classification process, the *Image Classification* toolbar was used. With the aid of the *Training Sample Manager*, the training samples were created, based on visual interpretation (Figure 7).

Figure 7: Example of training samples (green: vegetation, yellow: soil, purple: archaeology) .

After taking a look at the dendrogram and scatterplots (see results, p. 28) it was decided to create five classes (Table 3):

ID	Class name
1	Vegetation
2	Soil / Sparse vegetation
3	Tile roofs
4	Impervious surfaces / Roads
5	Archaeology / Stone features

Table 3: List of supervised classification classes.

Since land cover classification, at this stage, was focused on exposed architectural remains, further classification details of vegetation, were not needed. Thus training samples covered all vegetation areas without distinguishing, for example, between types of trees. After the training samples were defined, signature files were created, based on the pan-sharpened, composite Geoeye image, the pan-sharpened NIR, blue

and red bands and the NDVI. The blue band was included because it was observed as having higher reflectance for rock features in the composite image. The NDVI was included for detecting the vegetation. These signatures files were used in the final classification step. For this, the *Maximum Likelihood Classification* tool was used. Maximum Likelihood Classifier (MLC) is one of the most commonly used classification algorithms. It is based on the evaluation of variance and co-variance for each class in order to assign a pixel to one of them, according to highest probability (Lasaponara & Masini, 2012b). It calculates the probability of a pixel belonging to a class of those created, based on its spectral attributes, and the cell is assigned to that class that is most likely to belong to.

Unsupervised classification for excavated features

For unsupervised classification, the *Iso Cluster Unsupervised Classification* tool was used, again on the composite image, the blue, red and NIR bands and NDVI. The ISODATA (Iterative Self-Organizing Data Analysis Technique) algorithm is trying to create meaningful groups from computer-generated spectrally similar clusters. It merges or splits clusters if their centers are within a certain threshold or if a number of pixels are less or more of a certain threshold. In order to map exposed archaeological features, when running the tool, a different combination of number of defined classes, class size (number of cells in the class) and sample intervals (interval used for sampling) was used. It was observed that more accurate results were presented with the definition of 7 classes, an 18 pixels minimum class size and a 10-pixel sampling interval. The more the number of classes the more accurate the unsupervised classification gets but also more detailed. To further examine the results, and since the three classes were related to vegetation, results were reclassified, using the *Reclassify* tool, to four new classes (Table 4):

ID	**Class name**
1	Vegetation
2	Soil / Sparse vegetation
3	Archaeology /Rock
4	Impervious surface / Roads

Table 4: List of unsupervised classification classes.

Unsupervised classification for possible buried features

For testing the potential of unsupervised classification for investigating possible buried features, a different approach was followed. For this classification, the ISODATA algorithm was used again and the resulted vegetation indices were used as input data, namely NDVI, DVI, SAVI, MSAVI, SR, SQRT SR, MSR, ARVI and EVI. The classification of the vegetation indices results was executed entirely on vegetation fields so as to minimize variability of the clustered material. In order to achieve this, polygons were created from the vegetation classes from the previous supervised classification. Then, the resulted shapefile was used as a mask to extract the necessary areas from the different vegetation indices images.

The extracted fields were finally classified, using 2 classes, with an 18 pixels minimum class size and a 10-pixel sampling interval. The reason behind this experimentation was that by using two classes it would be easier to track changes in vegetation, since healthier areas would appear in one class and more apparent, unhealthy areas, as "anomalies" in the other class. The two classes were called "vegetation" and "anomalies".

4.2.3 Interpretation and validation

After the processing stage was completed, the interpretation and validation of the processed images followed.

Anomaly assessment

Following the most common method of interpretation in similar studies (e.g., Gennaro et al., 2019; Donati & Sarris, 2016), the derived vegetation indices were visually examined for the detection of linear or rectangular anomalies that could suggest the possible existence of archaeological features. These anomalies are expressed as differences in the general surrounding. For example, indications of stressed vegetation in a field with generally green plants. Possible anomalies were digitized as polylines and saved as new shapefiles, with an id number assigned and information added, regarding the indices where those features were more evident. After cross-examination with the existing dataset of known archaeological features in the area and modern fields, more information was added with regard to the potential nature of these anomalies, resulting to a narrower number of anomalies of possible archaeological nature.

Accuracy assessment

This process can be largely divided into three parts and entailed the creation of confusion matrices (see Appendices I-V).

For the mapping of exposed archaeological remains, an accuracy assessment was conducted for the supervised and the unsupervised classifications of the pansharpened composite image, the blue, red and NIR bands and the NDVI. As mentioned earlier, the Geoeye image, on which all processing was based, was acquired in 2012, which comes with the inability to be evaluated on the basis of up-to-date ground truth data collected in the field. For this reason, validation points were created on the same Geoeye image, based on visual interpretation, the cross-examination with the archaeological features shapefile and personal knowledge of the area. In total, 50 validation points for each class were randomly created. During the accuracy assessment, overall, producer and user accuracies were calculated. The validation points that were created had a class and land cover type assigned. Then values from the classified images were extracted to points and overlapped with the validation point shapefiles. Overall accuracy was calculated by dividing the sum of the correctly mapped points with the total number of validation points. Producer accuracy was calculated by dividing the sum of correctly mapped points with the total number of validation points. User accuracy was calculated by dividing the sum of correctly mapped points with the sum of map data points. For all the above accuracy assessments, the *kappa* coefficient was also calculated, using the following equation:

$$\kappa = Nd - q / N^2 - q$$

where *N* is the total number of validation points, *d* is the sum of correctly mapped points and *q* is the sum of products between the number of validation points and the number of map data points for each class.

The unsupervised classification of the vegetation fields, for tracking possible buried remains, was initially evaluated in accordance with the possible archaeological anomalies' shapefile, derived during the anomalies assessment. The possible archaeological anomalies polylines were turned into points and used as validation data. This resulted in 397 points that were used in the accuracy assessment of the two classes. Even though overall, user and producer accuracies were to be calculated, only overall accuracy can be taken into account because we have only two classes and points

concern only the “anomalies” class, user accuracy is always the same as overall and producer is always one. Through this approach, it was anticipated to observe not only the potential of unsupervised classification for monitoring possible buried features but also at what extent the visual interpretation process can be trusted, for the same purpose.

In two areas from those examined in the previous steps, there was the option to conduct an accuracy assessment of the unsupervised classification for possible buried features, by using more trustworthy reference data. One case was the “west of soccer field” area, for which the 63 GPS points that were collected along recently excavated walls were used as validation data. In the other case, for the Late Roman wall area, 53 validation points were created on the map, based on the georeferenced data from the 2001 geophysical survey. As was the case in the previous part of the analysis, only the overall accuracy was taken into account**.**

5. RESULTS

Classification for exposed features

Supervised and unsupervised classification were used for mapping exposed archaeological remains. Additionally, supervised classification was used as the basis for separating vegetation-only fields that were used later in the unsupervised classification of vegetation indices. Generally, both classification methods seem to provide fairly good results, regarding the production of land classes that involve exposed archaeological features, even if in many instances the spectral signatures are not very distinct.

Supervised classification

During supervised classification, spectral differences between remains of archaeological interest and other classes, apart from vegetation, prove to be very small. As mentioned earlier, five classes were created at this stage. The classification of the composite image, provided the best results (Figure 9). Usually, we can get the general outline of archaeological features but in many cases, these are confused with other classes. A look at the dendrogram and the spectral signatures (Figs. 8,10), shows that apart from vegetation, which is well separated, all other classes have quite short spectral distances.

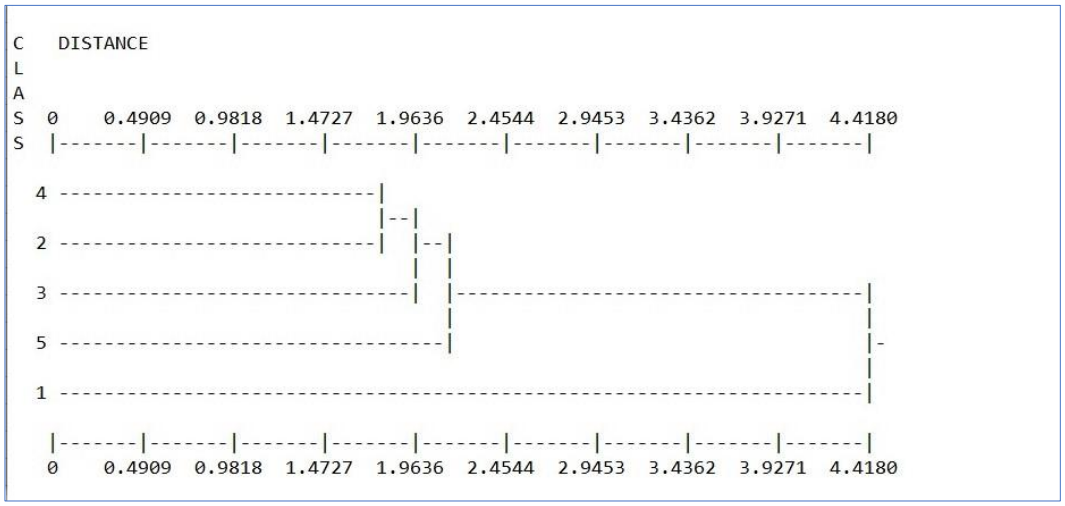

Figure 8: Dendrogram of classes created showing distance among values (1: vegetation, 2: soil/sparse vegetation, 3: tile roofs, 4: impervious surfaces, 5: archaeology/rock).

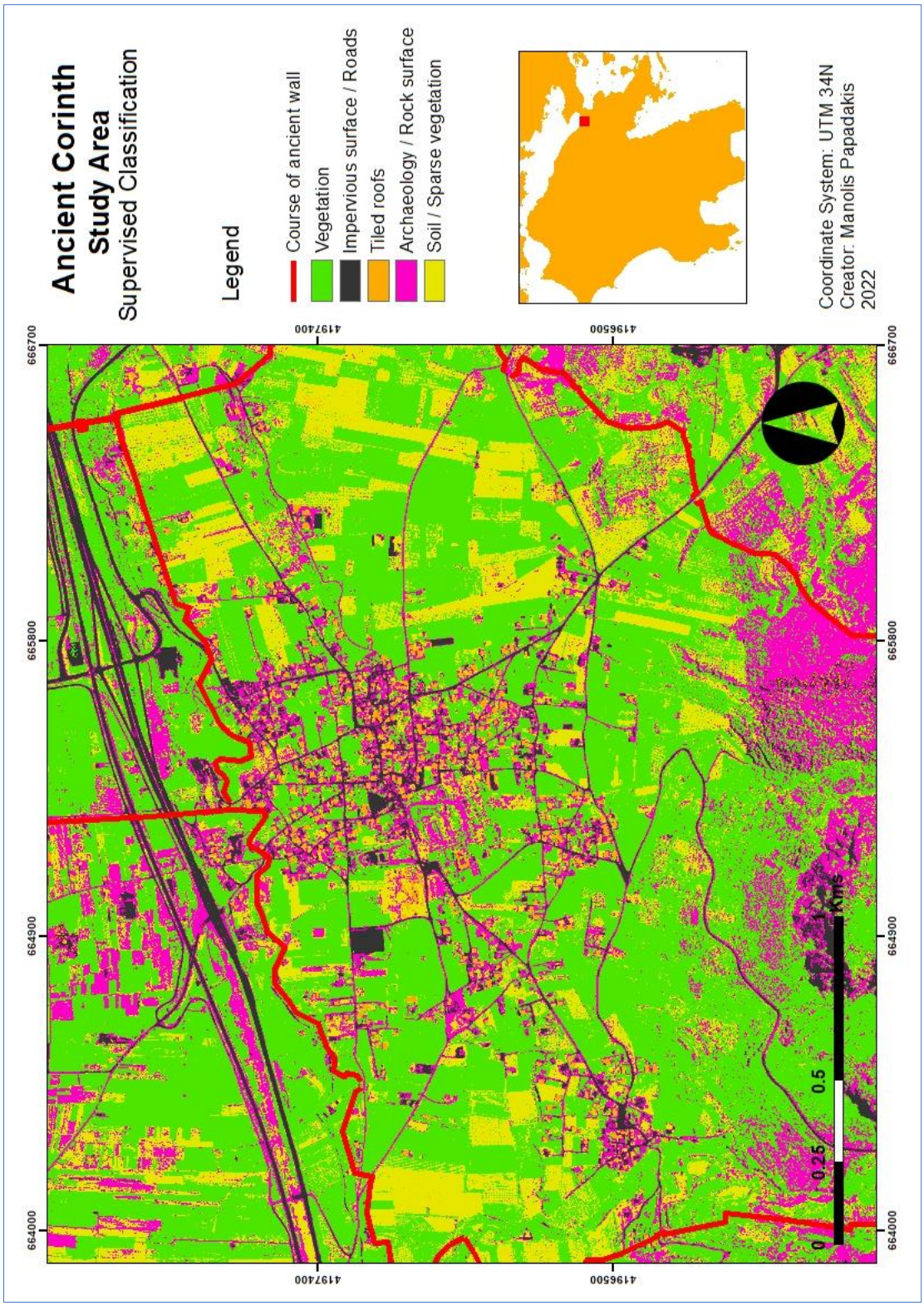

Figure 9: Supervised classification of composite image.

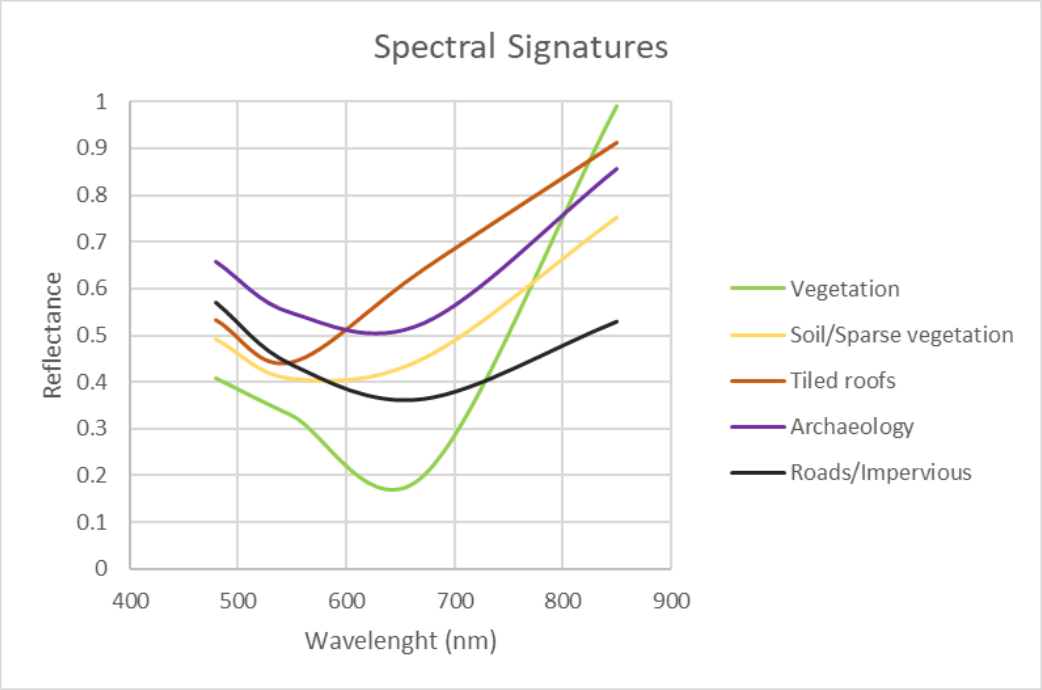

Figure 10: Spectral signatures of classes.

This is more apparent differences in the spectral signature between soil and tiled roofs and impervious surfaces, like concrete. Archaeological features, can be confused with soil and impervious surfaces and that can be normal since the material used and exposed is, almost always, stone or bricks. Through the confusion matrix, it can be observed that overall accuracy was very high at 92.4%, with vegetation being the most accurate class mapped with user accuracy at 100% and producer at 98.04%. Also, the *kappa* was at 0.9. Archaeology or rock features mapping provided also good results with user accuracy at 98% and producer at 76.56%. The rest of the classifications did not provide very good results, with only the blue band being comparatively better, with overall accuracy 58.8% and archaeology features user and producer accuracies at 62% and 42.47% respectively (Appendix IV).

Unsupervised classification

Unsupervised classification was used by defining 7 classes, which were later reclassified in four classes (see p.25). In many cases, this type of classification was successful in two ways: a) separating archaeological remains from other surrounding classes, which may cause confusion and b) in mapping with better detail at wall width. As in the supervised classification, the composite image yielded the best results (Figure 12). At one instance, it was possible to identify remains of some walls that were proved to belong to an excavation, taking place back in 2012, and which was not noticed before,

when examining the RGB image (Figure 11). After examining the error matrix, there was a 54.4% overall accuracy with vegetation being again the most accurately mapped class with 100% user accuracy and 98.04% producer. The rest of the classes were less accurately mapped, compared with supervised classification while the *kappa* was at 0.43. Archaeology and rock features provided 64% user accuracy and 39.51% producer. This class was quite mixed with the impervious surfaces and soil classes while the most distinct difference was the inability to map roof tiles separately as they were mixed with impervious and rock surfaces (Figure 13).

Figure 11: Detail of unsupervised classification, showing how the walls from excavation trenches were classified. Note also more south the detail of the classification of a Late Antique church in contrast with the surrounding vegetation.

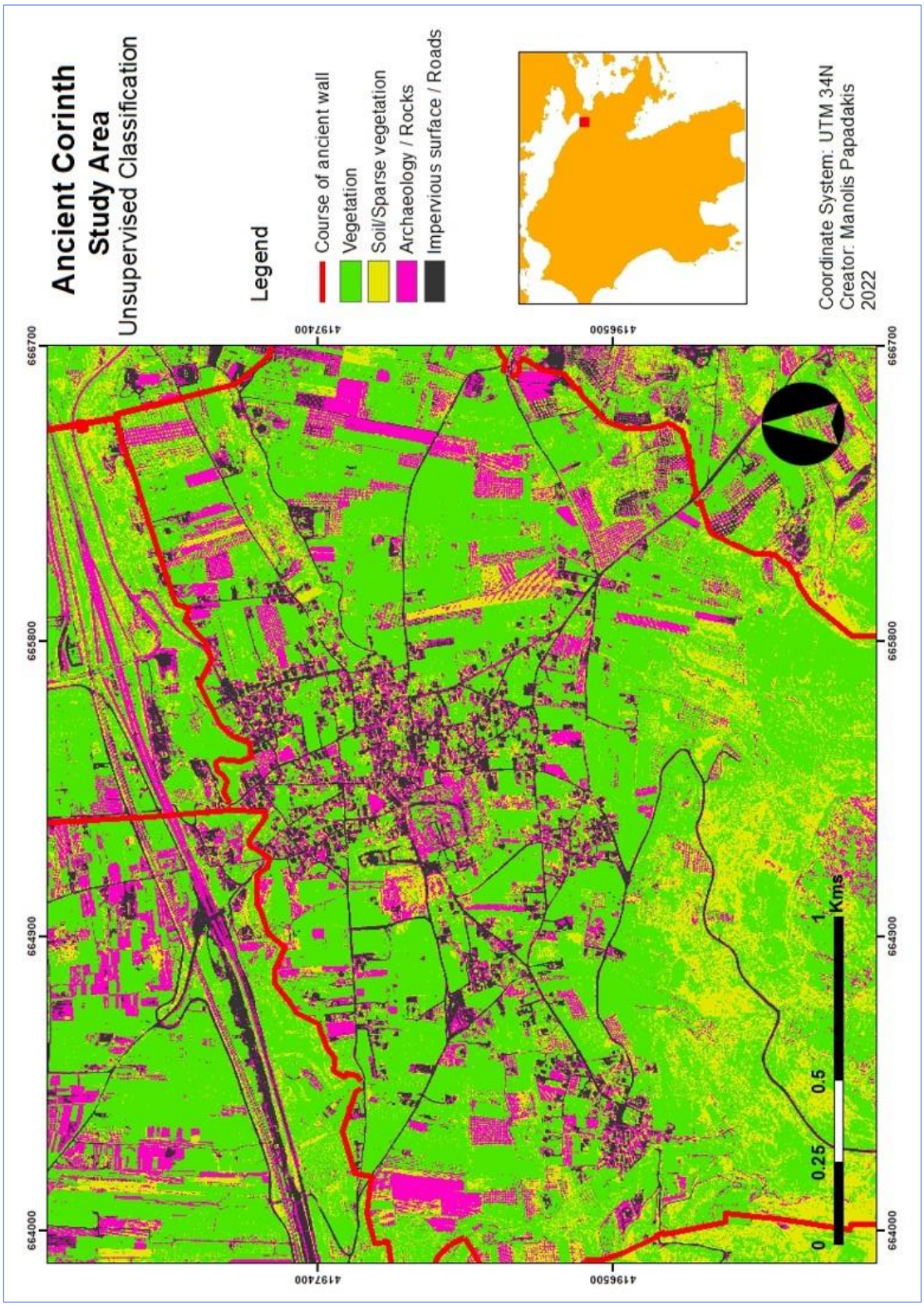

Figure 12: Unsupervised classification of composite image.

Figure 13: Dendrogram of classes created showing distance among values (1,3,5,6: vegetation, 2: soil/sparse vegetation, 4: archaeology/rock, 7: impervious surfaces).

The classification of the blue band provided a better overall accuracy of 55.6% but a less good user and producer accuracy of the archaeology features at 44% and 0.14%, respectively. The least good results were provided by NDVI, with overall accuracy 31.2% and archaeology features user and producer accuracies at 34% and 25.76% respectively (Appendix V).

Vegetation Indices

The photointerpretation, which followed the calculation of vegetation indices, was focused on the visual identification of anomalies that could indicate possible unknown, buried archaeological features. In an effort for an interpretation as unbiased as possible, those anomalies were firstly identified through close inspection of the enhanced images and were later examined in relation with the surrounding environment and juxtaposed with the shapefile of archaeological remains. Initially, there were 60 anomalies identified (Figure 16).

As all indices provide different results, not all of the anomalies were visible in every index. Most of the anomalies were able to be detected in a certain number of indices or through a combination. In general, NDVI seemed to be the most useful index during the interpretation process, providing help in observing 78% of the identified anomalies.

SAVI, DVI and MSAVI were also helpful in 45%, 45% and 42% of the detected anomalies respectfully. At the other end, ARVI and SQRT SR had the least satisfactory results, contributing to the detection of just 2% and 8% of the anomalies, respectively (Figure 14).

From all the anomalies detected, 11 could be more securely associated with features of archaeological interest, which may indicate buried walls or roads, based on the interpretation along with the archaeological features shapefile. At this stage, NDVI was proved to be the most useful index, contributing to the identification of ten of these 11 anomalies. These usually appear in linear or rectangular shapes and in some cases, they could be related to known archaeological remains or their potential extension in the landscape, as observed in the archaeological record (Figure 15).

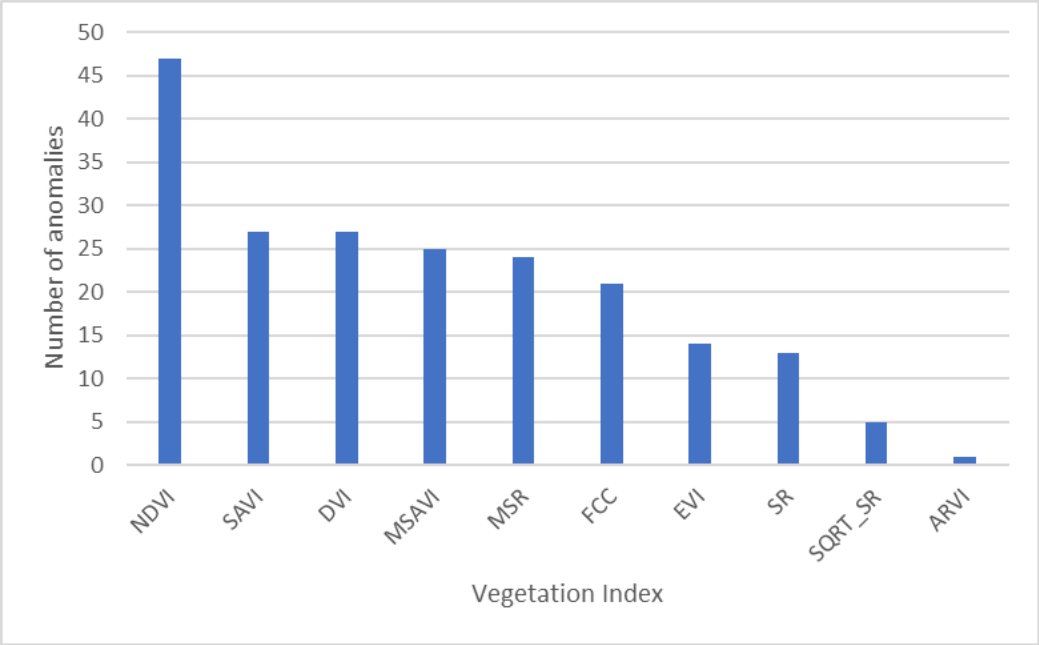

Figure 14: Number of anomalies identified per vegetation index.

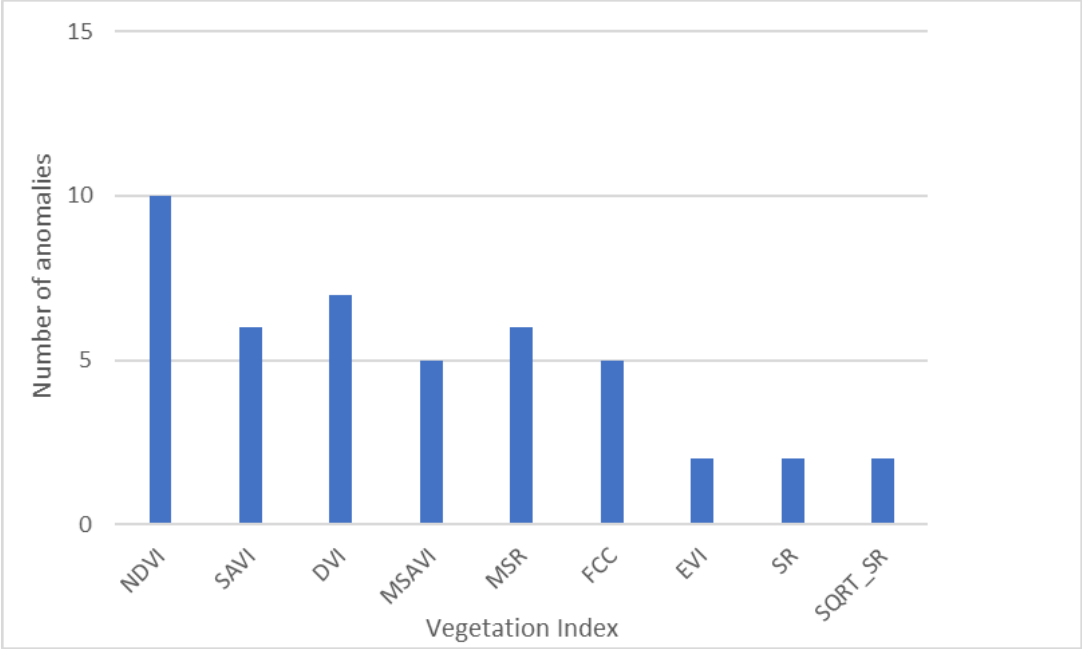

Figure 15: Number of possible archaeology anomalies identified per vegetation index.

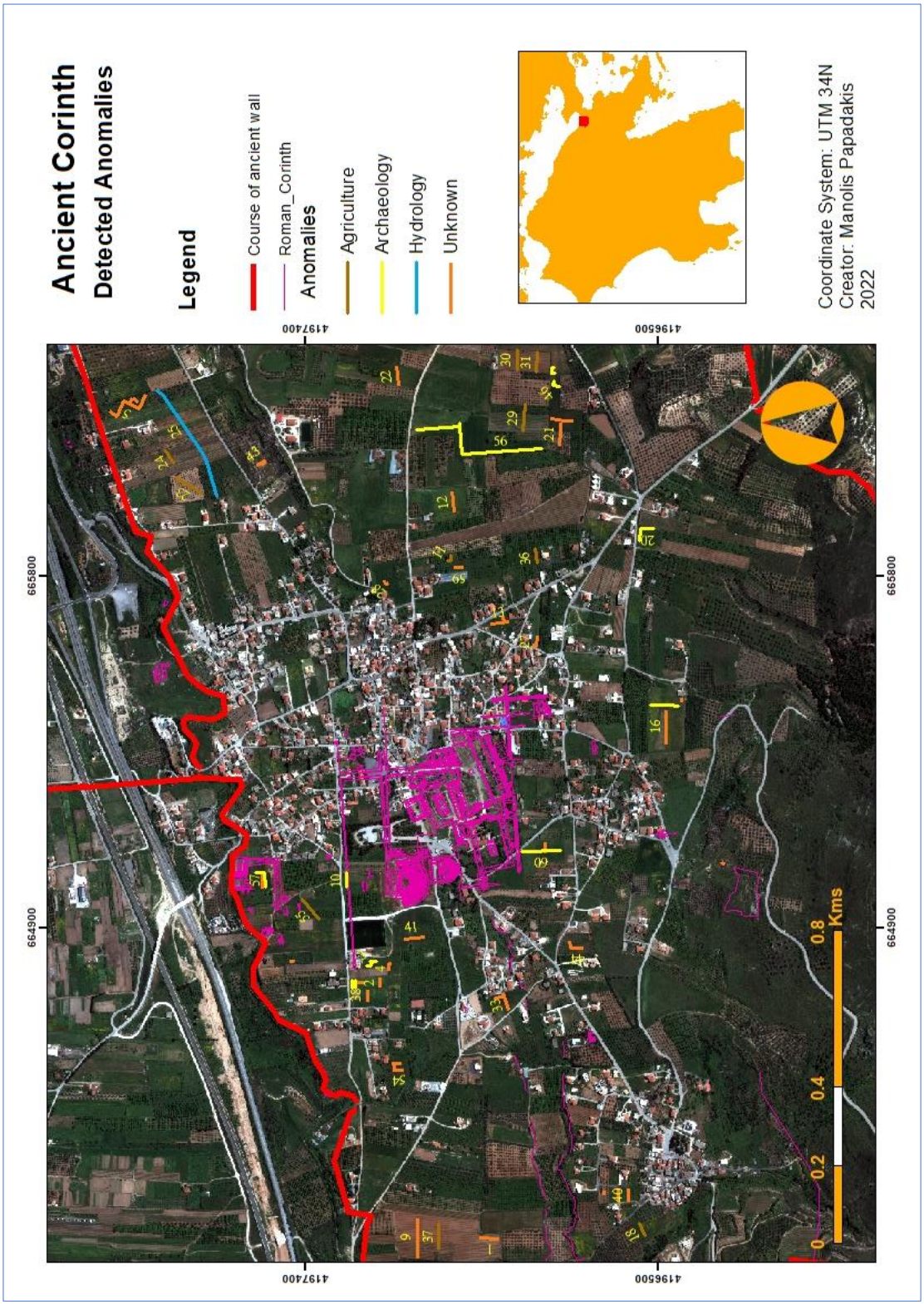

Figure 16: Detected anomalies.

More specifically, some anomalies (ID: 10, 50 and 51) are suspiciously aligning with the projected extension of an E-W road (decumanus). A closer look around anomalies 50 and 51 reveals a larger area of stressed vegetation, which could possibly lead to a more extended area of archaeological interest (Figure 17). West of the soccer field, anomaly 3 was identified, as a combination of linear and orthogonal lines. It was later noticed, that this anomaly appears in a field excavated in 2018 and so this area, after it was classified, was further evaluated with the GPS points gathered along the today exposed walls.

Figure 17: DVI index with Anomalies 3, 10, 50 and 51.

Another good candidate for a road feature could be anomaly 60, located south of the forum, extending 100m with a N-S direction (cardo) and almost parallel to another verified N-S road to its west. One of the more secure archaeological remains detected was anomaly 56, a long, zig-zag feature, extending for 386m, with a N-S direction. This anomaly falls directly on the supposed course of the Late Roman wall and part of it was also detected during the geophysical survey of 2001. For this reason, it was further evaluated with the geophysics data (Figure 18). Finally, anomaly 57, also had a very high probability of belonging to a building complex due to its location, directly among other known remains, comprised of a temple and a stoa (a covered walkway). Additionally, it seems to follow the orientation of the stoa, with a total length of approximately 61m (Figure 19).

Figure 18: NDVI index with Anomaly 56.

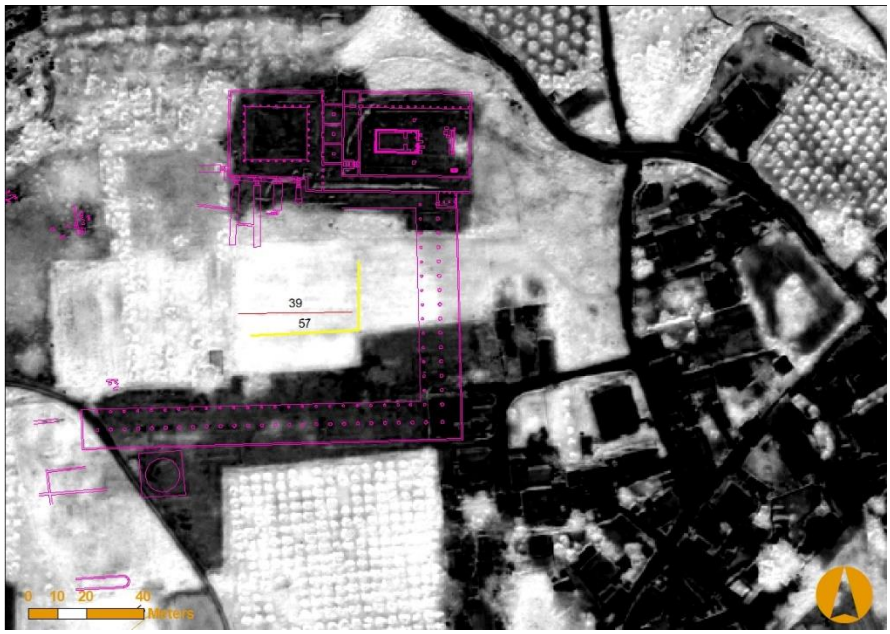

Figure 19: NDVI index with Anomaly 57 and archaeological features (purple).

Considering the rest of the anomalies, one could be associated with a hydrological feature, based on its shape and length. As Corinth was known for its dense hydrological network, comprising of rivers, streams and springs, this might be part of a paleochannel, meaning an old, now nonexistent river, which was filled with sedimentary deposits after it dried up (Upadhyay et al., 2021). Another 13 anomalies could be related to agricultural activity. This can include paths between fields, plough lines or former field borders. Anomaly 5 is a very conspicuous one but could not be inferred with certainty if it belongs to a possible wall complex or to paths being created in this particular field.

The remaining 35 anomalies are of unknown nature but without excluding the possibility of belonging to archaeological remains as well, even if they are not immediately related to known archaeological features. This is because some of these linear, unknown anomalies, as well as some of the agricultural ones, seem to follow a pattern that could indicate some relation to past activity. A short study of their alignment shows that many of them follow a W-E or N-S orientation (85^{o}-95^{o} and 175^{o}-185^{o} angle respectively), corresponding to the ancient urban planning of the city, which was dictated by the cardinal points. Moreover, some of those anomalies run parallel to others nearby, in some places at equal intervals, indicating possible traces of buried streets or other remnants of the ancient grid system.

Unsupervised classification for possible buried features

In order to examine the potential of automated classification techniques for the identification of possible buried features, unsupervised classification was conducted for the eight vegetation indices. After the classification was finished, two classes were created, one indicating healthy vegetation and one changes in vegetation (anomalies), which, in some cases, could be related with possible, buried archaeological remains. During the accuracy assessment, the classification was used in conjunction with the 11 possible archaeological anomalies identified in the previous step. Even though overall, user and producer accuracies were to be calculated, only overall accuracy can be taken into account. Because we have only two classes and the validation points extracted from the 11 anomalies concern only the "anomalies" class, user accuracy is always the same as overall and producer is always one (Appendix I). According to the error matrix, the classified changes in vegetation cannot be securely associated with the anomalies, visually identified from the vegetation indices. The best association between them and the classification, was when using NDVI (Figure 21), with an overall accuracy of 41.06% and MSAVI, with 38.29%. On the opposite end, MSR provided the poorest accuracy, with 7.05% (Figure 20).

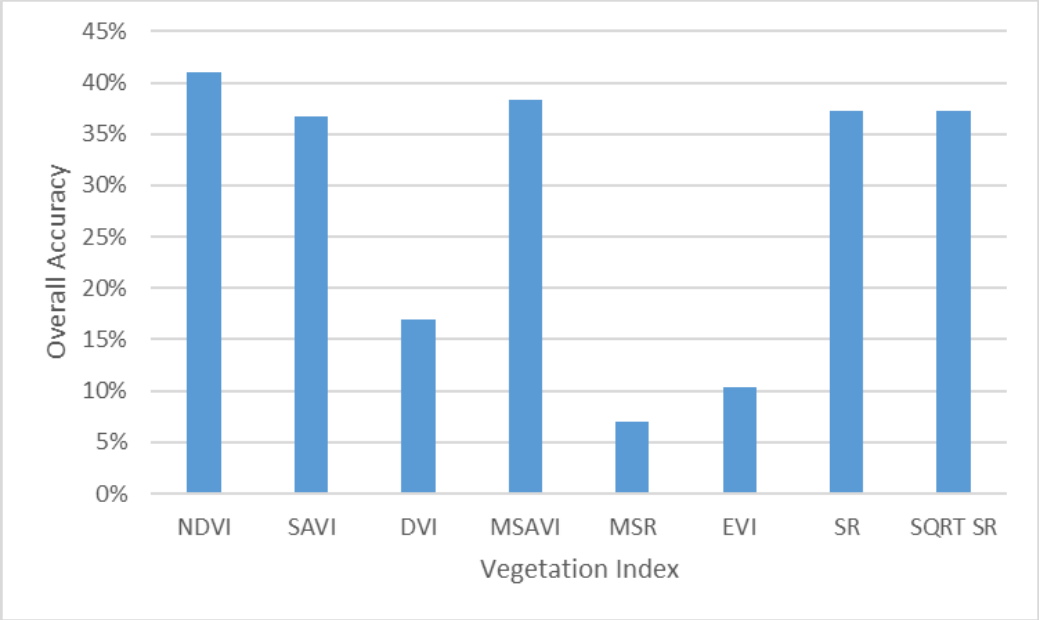

Figure 20: Overall accuracy per vegetation index for unsupervised classification of general study area.

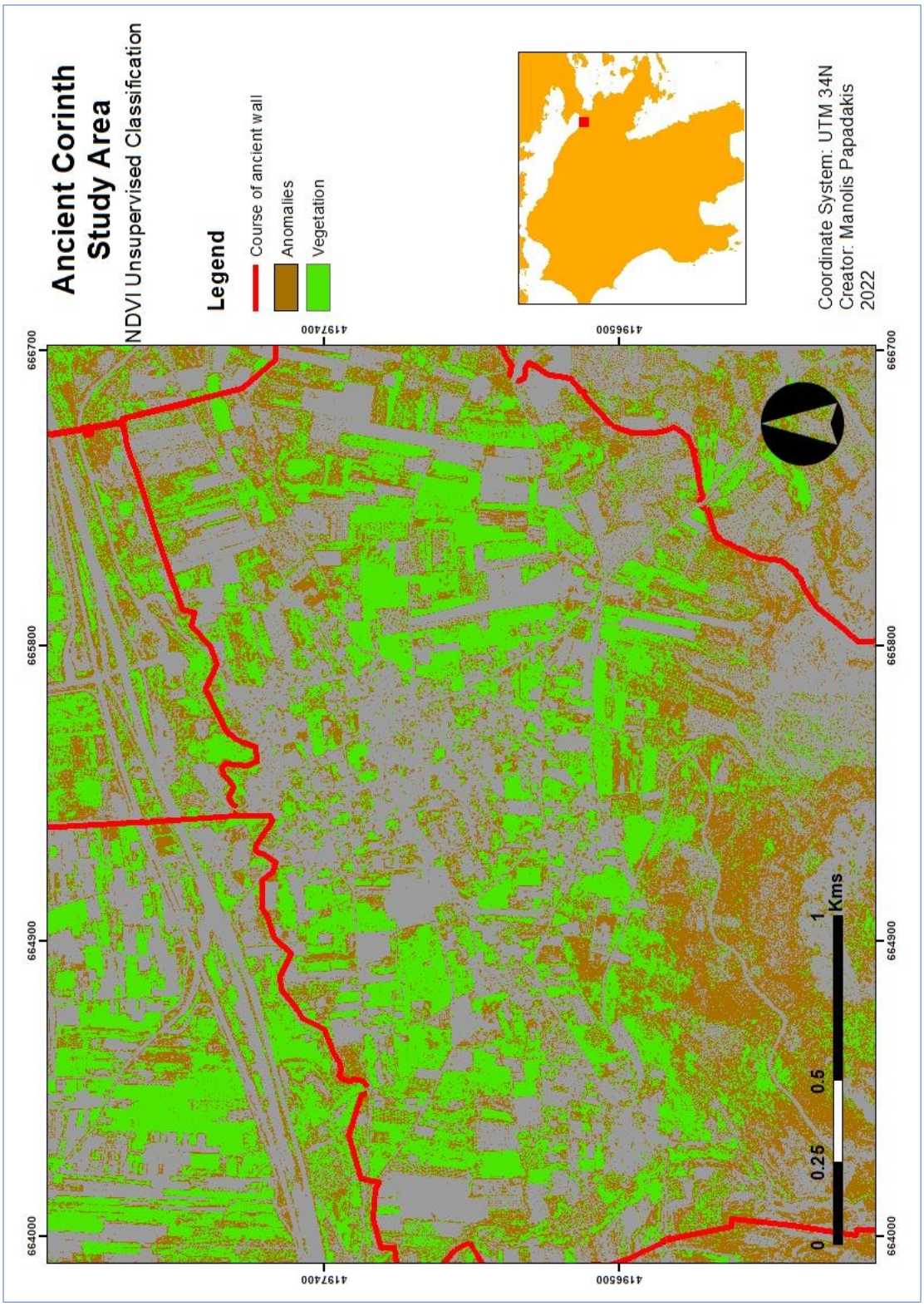

Figure 21: Unsupervised classification of NDVI.

As mentioned earlier, in two cases, there was the opportunity to test the classification results with more up to date ground truth data from two areas. In both those areas, possible archaeological anomalies had been visually identified from the vegetation indices. In the first case, the accuracy assessment was conducted for the area west of the soccer field, where anomaly 3 was identified (Appendix II). The confusion matrix showed a very low overall accuracy for all classified images. Most of the classified maps showed a 12.7% overall accuracy, with only DVI providing better results, with 23.81% accuracy (Figure 22).

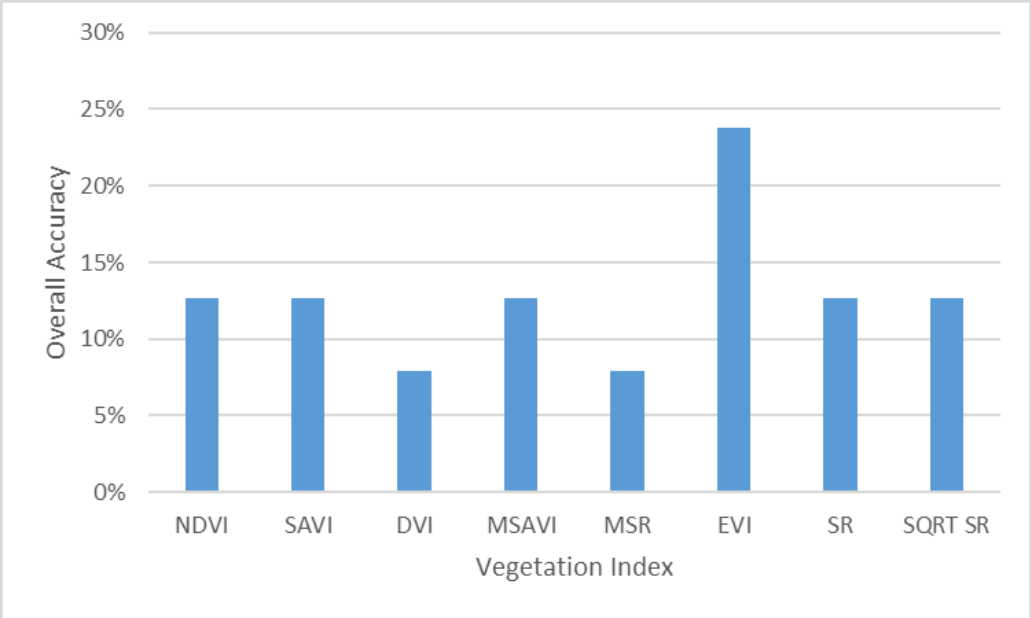

Figure 22: Overall accuracy per vegetation index for "west of soccer field" area.

In the second case, the accuracy assessment was conducted at the possible course of the Late Roman wall, which was also identified as anomaly 56. In this case, the accuracy results were slightly more promising (Appendix III). Overall accuracy was improved for all classified indices, with NDVI and MSAVI providing the best accuracy with 47.17%. The poorest overall accuracy was provided by MSR, with 15.09% (Figures 23,24).

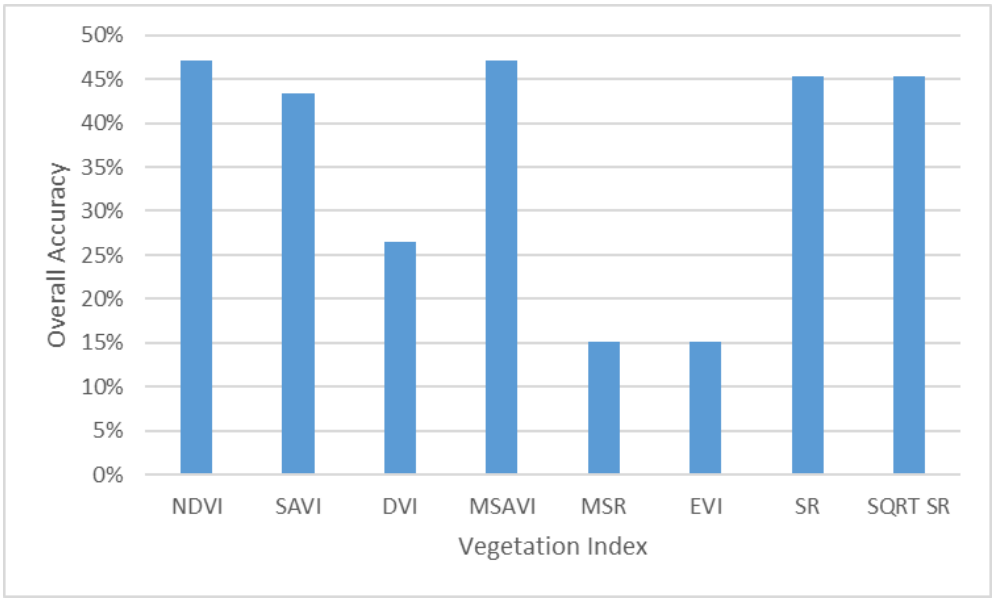

Figure 23: Overall accuracy per vegetation index for the Late Roman wall area.

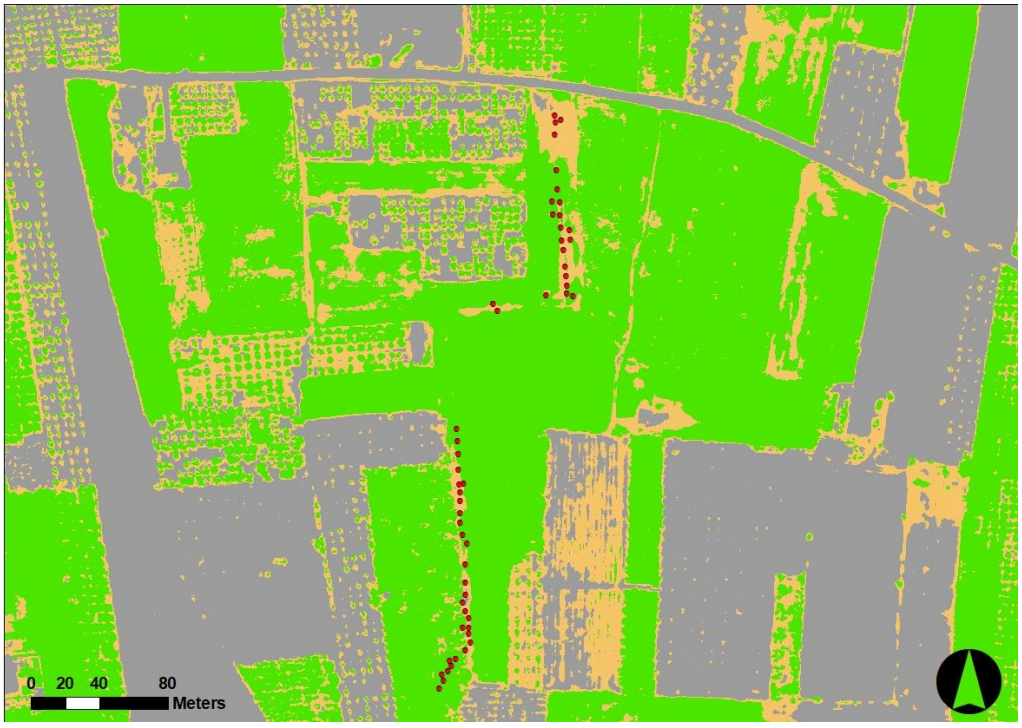

Figure 24: Late Roman wall area, NDVI classification with validation points.

6. DISCUSSION AND FUTURE RESEARCH

Visual image interpretation has long been a common method within archeology for retrieving information from remotely sensed imagery (Lasaponara & Masini, 2012d). Based on the subjective perspective of the interpreter, which can be shaped by their training, experience and knowledge of an area, a number of on-surface features or phenomena can be recognized, at the time of data acquisition. Subsequently, characteristics, such as size, shape, pattern or texture, can indicate the presence of certain features. However, most of the times, and in particular when investigating targets of archaeological interest, interpretation results cannot be fully evaluated.

The site of Ancient Corinth, has been under investigation and excavation for over a century now, and this gives us the opportunity to exploit an established archaeological record in order to evaluate techniques that have been widely used in archaeological remote sensing. The photointerpretation results, based on vegetation indices and the classification methods, were thereby possible to be compared with the already existing archaeological record in order to test their validity.

It is shown through the results that, to some extent, this was possible. In many similar studies, the observation of anomalies in spectral signatures, in relation with the surrounding areas, cannot be evaluated (e.g., Gennaro et al., 2019; Donati & Sarris, 2016). The manipulation of vegetation indices may reveal some discrepancies in spectral signatures, which can only be inferred to belong to archaeological features through the examination of their characteristics, as mentioned above, and the archaeological history of the region. However, in the case of Ancient Corinth, the juxtaposition of the detected anomalies with known features helped in narrowing down potential archaeology candidates and the use of unsupervised classification provided a way to evaluate them, regarding at least a number of them. As a result, some of the anomalies did correspond to archaeological features, known and in some cases attested through excavations and surveys.

During the visual interpretation process, some indices appeared to provide more promising results compared to others, making the identification of anomalies easier. NDVI was particularly helpful for discerning subtle details in vegetation and in some cases, it was enough by itself for the recognition of those anomalies. Nevertheless, the

observation of two or more indices, usually including MSAVI, SAVI and DVI, was helpful in identifying features that were either partly or not visible in other indices and cross-checking those, which could be observed in more than one index. This could be potentially caused by the fact that some indices, like EVI, perform better in regions with higher biomass (Luz et al., 2022) while Ancient Corinth is more scarcely vegetated. The identification of anomalies though does not come without drawbacks and limitations.

Firstly, the varied vegetation and density of trees renders difficult to discern differences at ground level. During the last 60 years, the intensification of agriculture has led to the planting of different kinds of trees, which cover much of the unexplored areas and share different phenological cycles. Signs of stress caused by buried features are prone to be more apparent in the examination of low and more uniform vegetation, such as wheat fields or natural weeds, rather than in tree canopies. In this respect, it is worth mentioning that all of the anomalies detected during this study were placed in fields with low vegetation. Furthermore, the cultivation practice of planting trees at regular intervals may create a false “grid” effect, between green vegetation and exposed soil, which can be amplified by tracks for modern transport between the trees and give the impression of anomalies (Figure 25).

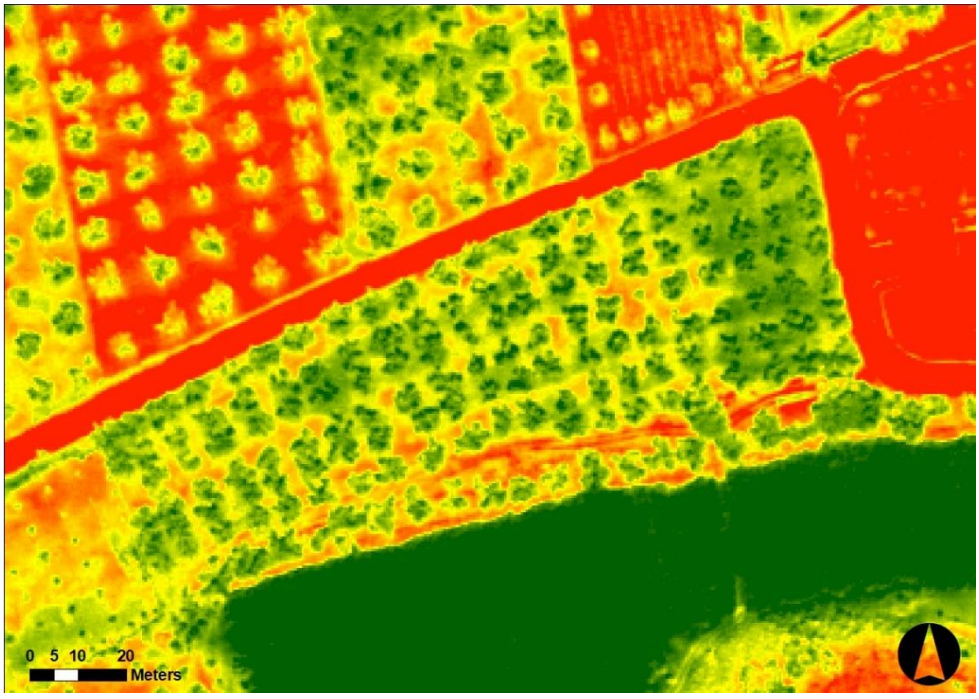

Figure 25: Example of "grid effect" between vegetation and exposed soil, due to trees arrangement.

Secondly, the site of Ancient Corinth has been continuously inhabited for many centuries and grown into a semi-urban area, leading to disruption of archaeological evidence. Buildings and roads have been altered before getting destroyed and the grid plan of the city has been modified and possibly, in certain places, being in use until today. This situation seems to be particularly present in some of the field boundaries observed, which may cause a confusion in the identification of anomalies. As a result, this further limits our ability to associate anomalies in vegetation signatures with archaeological features. In contrast with sites that may have not experienced continuous occupation and where a clear assumption on the nature of the possible archaeological features could be made, in Corinth, it proves more difficult to identify if the anomalies may belong, for example, to a road or wall, let alone to determine their chronological phase.

Unsupervised classification, due to its ability to automatically distinguish spectral differences, can be used in a complementary way in order to cross check visually interpreted anomalies from vegetation indices and to track changes in vegetation, which could be promising for future archaeological research. However, this process should not be followed without caution. In some cases, there was an overlap of the identified anomalies with classified areas of "stressed" vegetation but according to the accuracy assessment results, not at an extent that can be fully trusted, meaning an accuracy of at least 70%-80%. When assessing the classification results with data collected from known features again the accuracy was at low level (Appendices II, III) However, in both cases, there was indication of stress in the vegetation that was captured during the unsupervised classification process. More interestingly, the results were better regarding the Late Roman wall. That may happen since in this case the wall width is expected to be larger (approx. 1-3m), compared with the walls that were excavated west of the soccer field (approx. 0.7-1m.). A larger wall width should cause bigger stress on the vegetation above and also less detail is needed when mapped, because of its extent. Comparatively, the NDVI and MSAVI seemed to be the more promising indices for similar, future studies.

In general, supervised and unsupervised classifications proved helpful in mapping exposed architectural remains. However, only the composite images, in both cases, provided satisfactory results. The single bands (blue, red, NIR) did not prove very useful while the experimentation with the NDVI showed that probably vegetation

indices are also not suitable for exposed built features. Supervised classification offered very high overall accuracy and at the archaeology class. Unsupervised classification was less accurate but at an acceptable level to be advised. On one hand, supervised classification offers the ability to differentiate between classes that share similar characteristics in order to create more accurate clusters. This, for example, was the case of the differentiation between soil and tiled roofs. The control in defining classes through training samples can, in some cases, guarantee the correct assignment of a class on certain features but not throughout the whole mapped area. On the other hand, unsupervised classification seems to have an advantage in revealing discriminable objects even at smaller sizes. As a result, walls and archaeological features were differentiated in a more satisfactory way. This advantage helped in the identification of exposed features that had not been earlier observed, thus, rendering unsupervised classification, a promising technique for the detection of unknown aboveground features that are difficult to notice in the first place, especially when there is a sharp difference in spectral signatures (e.g., a wall among wild vegetation).

Classification methods and pattern recognition, using satellite data, for archaeology and cultural heritage is a quite recent research topic and the available classification techniques, offered in a GIS environment, may not be fully adequate for the classification of very-high resolution images. Our goal was to map not general areas of archaeological interest, where standing features are present but specific remains that can have sub- or around-meter width. These usually blend with surrounding features that could be grown vegetation, soil or rocks. Even more, the material, which archaeological structures are made of or that is used for their restoration, is almost always rock or bricks. This condition causes a blend that appears as an overlap of spectral signatures, which in turn can impose an extra difficulty level in the classification process. During supervised classification, MLC depends on the assumption that pixels are “pure”, meaning representing only one class but this is not always the case, depended on spatial resolution. Similarly, in unsupervised classification, some spectral clusters may be related to mixed classes of material and therefore being physically meaningless in research that demands a high spatial resolution.

During this thesis, a number of limitations were present since the beginning and mistakes were noticed while progressing. These can fuel further discussion related to

the future of research and pertaining to not only the methods used but also the study approach to Corinth and areas with similar physical characteristics.

The use of very-high resolution satellite imagery for the detection of subtle anomalies in vegetation indices and classification is indispensable. However, the high cost of their acquisition can be restrictive for small scale studies, such as this current one. This was the reason only one such imagery set was used here. For a more complete study of the phenological cycles, imagery with a higher temporal resolution is needed in order to cover more seasons. Moreover, depending on the climatic conditions of each year, some features may be better discernible on one year but not the other. A complete record of available archaeological and other ancillary data (DEMs, soil maps, contours, previous surveys etc.) will always be useful to in order to validate results, monitor changes or, in case of predictions, to narrow down the possibilities. In order for this study to be more complete and to fully evaluate the potential of these processes for identifying buried features, a more complete record of excavated and investigated remains should be available so that is employed in an accuracy assessment.

Next to this, we need to consider the extensive tree coverage of the unexplored areas and the utilization of other methods and techniques. Synthetic Aperture Radar (SAR) has been used before in cases where the vegetation canopy is denser, since microwave wavelengths can allow deeper penetration and be more sensitive to surface morphology (Lasaponara & Masini, 2013). Light Detection and Radar (LiDAR) is another popular method, which can be used for mapping vegetation height and surface morphology for the detection of subsurface features, through the transmission of laser light at varied wavelengths (Raun et al., 2018; AOC, 2015).

The need for more recent very-high resolution imagery is also imperative for the classification process of exposed archaeological remains. When using classification for buried features, time acquisition of the image may be not that important. In some cases, it can even prove to be beneficial. However, for the classification of exposed remains, this can create difficulties during the validation process and the creation of an error matrix, based on up-to-date ground truth data. Since the imagery used here was extracted in 2012, an actual accuracy assessment, including sample points in the field, was not possible. In the last decade, land cover has changed, more areas have been excavated and architectural remains exposed while excavated areas, which appear

cleaned in the 2012 image, they have been now covered with vegetation or backfilled. So, even though an earlier image can be an advantage for the validation of results, regarding buried features, it also constitutes a major drawback for the accuracy assessment of classification of exposed remains. The alternative, which was followed here, is to create validation points, based on the 2012, Geoeye image but in this case validation and study data are the same. So, even though this is a method that has been used before (Ramzi, 2015), it is generally not suggested. Another alternative could be the use of other, more recent satellite imagery, which can be acquired free of charge. However, available, freely-distributed satellite images do not comply with the spatial resolution needed for classification at wall level (e.g., Landsat can offer a maximum 15m resolution and Sentinel 10m resolution). Consequently, only the purchase of a recent VHR image would be an appropriate solution.

The use of GIS for the collection, analysis and interpretation of spatial digital data is a growing trend in archaeological practices. The accessibility to a wide selection of GIS and image processing software (e.g., ArcGIS, ERDAS Imagine, ENVI) has given archaeologists the ability to integrate diverse data in order to predict locations of archaeological interest, manage existing excavations, monuments and future development works and monitor changes in the landscape. For all these purposes, satellite remote sensing is becoming more and more useful as a non-destructive, research tool.

7. CONCLUSION

In this study, there was an effort to evaluate different processing methods of VHR multispectral imagery for archaeology and cultural resources management and at the same time to contribute to the archaeological research of Ancient Corinth. It was shown that established techniques and processes can enhance the investigation and mapping of undiscovered, buried and exposed archaeological remains. However, results should always be treated with caution and further validation is always necessary, when possible.

Through the manipulation of different vegetation indices, based on the visible and NIR spectra, it was possible to detect subtle changes on the vegetation cover of the study area. Regarding which indices can be more helpful in this respect, even though a combination of indices was preferred, acting complementary to each other, NDVI was the most consistent one for detecting these anomalies. However, to what extent someone can be certain about their nature and whether they belong to buried archaeological features, it depends on further validation of data and association with other known features. For this purpose, unsupervised classification, could provide some further guidance, through accuracy assessment, but results should always be validated in order to reach concrete conclusions.

In the case of Ancient Corinth, it was possible to associate some of these anomalies with known remains and archaeological data in order to increase the possibility of identifying some of them as of archaeological nature. Most of these anomalies seem to belong to roads, with a few of them being part of a major E-W road, while others were identified as parts of a Late Roman wall. Nevertheless, it should be noted that no matter how detailed a validation can be, the only way to actually verify these sorts of results would be through further archaeological investigation, meaning excavations or geophysical surveys (Gron et. Al, 2011). At the very least, here, we get a good impression of the density and location of possible archaeological features.

Regarding their effectiveness in mapping features, supervised and unsupervised classifications, proved effective for mapping exposed archaeological features with certain limitations. These lie with the material of the features itself and the inability to differentiate from surrounding material that shares similar spectral properties, such as rocks and soils. However, archaeology related clusters may be more distinctive when

surrounded by vegetation, where spectral overlap can be smaller and, in these cases, we can map archaeological remains even at wall width. In particular, unsupervised classification, when setting appropriate parameters (number of bands, pixel size), can be a promising technique for identifying remains that would probably not be noticed in a regular RGB image. Moreover, through the juxtaposition with the anomalies discovered in vegetation indices, unsupervised techniques showed promising potential for the use of mapping buried features as well.

All in all, when using the methods and techniques presented in this study, one has to bear in mind the challenges related to the study of regions like Ancient Corinth, stemming from their diverse environment, product of continuous occupation and in relation with the nature of archaeological material. A lot depends on the visual ability, training and knowledge of the interpreter while any remote sensing technique should always be supplemented by field observations and adequate field surveys and ground truth data.

REFERENCES

Agapiou, A. (2020), "Evaluation of Landsat 8 OLI/TIRS Level-2 and Sentinel 2 Level-1C Fusion Techniques Intended for Image Segmentation of Archaeological Landscapes and Proxies", *Remote Sens*., 12(3), 579, https://doi.org/10.3390/rs12030579

Agapiou, A. and Lysandrou, V. (2015) "Remote sensing archaeology: Tracking and mapping evolution in European scientific literature from 1999 to 2015", *J. Archaeol. Sci*., Reports: 4, pp. 192-200

Agapiou, A., V. Lysandrou, D.Alexakis, k. Themistocleous, B. Cuca, and A. Argyriou. (2015) "Cultural Heritage Management and Monitoring Using Remote Sensing Data and GIS: The Case Study of Paphos Area, Cyprus." Computers, Environment and Urban Systems Journal 54: 230–339.

Agapiou, A., Alexakis, D. D., Sarris A. and Hadjimitsis D.G. (2014) "Evaluating the Potentials of Sentinel-2 for Archaeological Perspective", *Remote Sens*. 6(3), pp. 2176-2194

Agapiou¸, A., D. G. Hadjimitsis, A. Sarris, A. Georgopoulos, and D. D. Alexakis. (2013) "Optimum Temporal and Spectral Window for Monitoring Crop Marks Over Archaeological Remains in the Mediterranean Region", *Journal of Archaeological Science*, 40, pp. 1479–1492

Agapiou, A., Hadjimitsis, D.G., Georgopoulos, A., Sarris A., Alexakis D.D. (2012) Towards an Archaeological Index: Identification of the Spectral Regions of Stress Vegetation due to Buried Archaeological Remains. In: Ioannides M., Fritsch D., Leissner J., Davies R., Remondino F., Caffo R. (eds) *Progress in Cultural Heritage Preservation*. EuroMed 2012. Lecture Notes in Computer Science, vol 7616. Springer, Berlin, Heidelberg. https://doi.org/10.1007/978-3-642-34234-9_13

Aggarwal, S. (2004a) "Principles of Remote Sensing", in M.V.K. Sivakumar et al. (eds.), *Satellite Remote Sensing and GIS Applications in Agricultural Meteorology*, WMO, Switcherland, pp. 23-38

Aggarwal, S. (2004b) “Earth Resources Sattelites”, in M.V.K. Sivakumar et al. (eds.), *Satellite Remote Sensing and GIS Applications in Agricultural Meteorology*, WMO, Switcherland, pp. 39-66

Alexakis, D., Sarris, A., Astaras, T., Albanakis, K. (2009) “Detection of Neolithic settlements in Thessaly (Greece) through multispectral and hyperspectral satellite imagery”, *Sensors*, 9.2, 1167-1187

AOC Archaeology Group (2015) *An Introduction to LiDAR for Archaeology*

Arnoldus-Huyzendveld, A. & Citter, Carlo. (2014) “Site location and resources exploitation: Predictive models for the plain of grosseto”, *Archeologia Medievale*, 41, pp. 65-78

ASCSA (2022) https://www.ascsa.edu.gr/excavations/ancient-corinth/digital-corinth/maps-gis-data-and-archaeological-data-for-corinth-and-greece

Barker, P. (1993) *Techniques of Archaeological Excavation (third edition)*. London: B.T. Batsford

BSA (2022) https://www.bsa.ac.uk/about-us/library/collections_and_resources/aerial-photographs/

Campbell, B. J. and Wynne H. R. (2011) *Introduction to Remote Sensing*, 5th edition, New York: The Guilford Press

Canilao, M.A.P. (2017) “WorldView2 satellite imagery in remote sensing a past gold trading trail in Luzon: Testing ethnohistory-based and GIS-based models”, *Journal of Archaeological Science: Reports*, 12, pp. 363-377

Casana, J. (2020) “Global-Scale Archaeological Prospection using CORONA Satellite Imagery: Automated, Crowd-Sourced, and Expert-led Approaches”, *Journal of Field Archaeology*, 45, pp. 89-100

Champion, S. (1980). *A Dictionary of Terms and Techniques in Archaeology*, London: Morisson and Bibb Ltd

Chapman, H. (2006) *Landscape Archaeology and GIS*, The History Press, Gloucestershire, UK

Chen J. (1996) "Evaluation of vegetation indices and modified simple ratio for boreal applications", *Canadian Journal of Remote Sensing*, 22, pp. 229–242

Ciminale, M., Gallo, D., Lasaponara, R. and Masini, N. (2009) "A Multiscale Approach for Reconstructing Archaeological Landscapes: Applications in Northern Apulia (Italy)", *Archaeological Prospection*, 16, pp. 143 – 153

Corrie, R.K. (2011), "Detection of ancient Egyptian archaeological sites using satellite remote sensing and digital image processing", in Proceedings of SPIE, 8181, Earth Resources and Environmental Remote Sensing/GIS Applications II, 81811B (26 October 2011); https://doi.org/10.1117/12.898230

Cowely, D.C., Standring, R.A. and Abicht, M.J. (eds) 2010, *Landscapes through the lens. Aerial photographs and historic environment*, Oxford, Oxbow Books

European Space Agency. (2022, December 6). GeoEye-1. Earth Online. Retrieved April 5, 2023, from https://earth.esa.int/eogateway/missions/geoeye-1

Gamble, C. (2004) *Archaeology: The Basics*, London: Rutledge

Garrison, T., Houston, S., Golden, C., Inomata, T., Nelson, Z. and Munson, J. (2008) "Evaluating the use of IKONOS satellite imagery in lowland Maya settlement archaeology", *Journal of Archaeological Science*, 35, pp. 2770-2777

Gennaro, A, Candiano, A, Fargione, G, Mangiameli and M, Mussumeci, G. (2019) "Multispectral remote sensing for post-dictive analysis of archaeological remains. A case study from Bronte (Sicily)" *Archaeological Prospection*, 26, pp. 299– 311

Giardino, M. and Haley, S. B. (2006) “Airborne Remote Sensing and Geospatial Analysis”, in Jay K. Johnson (ed.), *Remote Sensing in Archaeology: An Explicitly North American Perspective*, The University of Alabama Press, pp. 47-77

Grøn, O., Palmér, S., Stylegar, F-A., Esbensen, K., Kucheryavskiy, S. and Aase, S. (2011) “Interpretation of archaeological small-scale features in spectral images” *Journal of Archaeological Science*, 38, pp. 2024-2030

Hadjimitsis, D.G., Agapiou, A., Themistocleous, K., Alexakis, D.D. and Sarris, A. (2013) “Remote Sensing for Archaeological Applications: Management, Documentation and Monitoring”, in Hadjimitsis D.G. (ed.), *Remote Sensing of Environment. Integrated Approaches*, InTech, Rijeka, pp. 57-95

Hayworth, C.L. (2003) “Geology of Corinth”, *Corinth XX, Corinth the Centenary 1896-1996*, pp. 15-40

Huete A.R. (1988) “A soil adjusted vegetation index (SAVI)”, *Remote Sensing of Environment*, 25, pp. 295–309

ITC, Jansen L.F and Huurneman G.C. (2001), Principles of Remote Sensing, An introductory textbook, ITC-Enschede

Jordan, C.F. (1969) “Derivation of Leaf Area Index from Quality of Light on the Forest Floor”, *Ecology*, 50, pp. 663-666

Kalayci, T., Lasaponara, R., Wainwright, J. and Masini, N. (2019) “Multispectral Contrast of Archaeological Features: A Quantitative Evaluation” *Remote Sensing*, 11(8), 913, https://doi.org/10.3390/rs11080913

Kalayci, T. (2016) “Settlement Sizes and Agricultural Production Territories: A Remote Sensing Case Study for the Early Bronze Age in Upper Mesopotamia.” *STAR: Science & Technology of Archaeological Research*, 2, pp. 217–234

Kaufman, Y.J. and Tanre, D. (1992) “Atmospherically resistant vegetation index (ARVI) for EOS-MODIS”, *IEEE Transactions on Geoscience and Remote Sensing*, 30, pp. 261–270

Kumar, G. (2019) “An Image Processing Tool to Generate Ground Truth Data from Satellite Images using Deep Learning”, Online, Accessed 25 Sept. 2022

Laben, C.A. and Brower, B.V. (2000) “Process for Enhancing the Spatial Resolution of Multispectral Imagery Using Pan-Sharpenin”, U.S. Patent 6,011,875, 4 January 2000

Laet, V., Paulissen, E., Meuleman, K. and Waelkens, M. (2009) “Effects of image characteristics on the identification and extraction of archaeological features from Ikonos-2 and Quickbird-2 imagery: Case study Sagalassos (southwest Turkey)”, *International Journal of Remote Sensing*, 30, pp. 5655-5668

Lambers, K. (2018) “Airborne and Spaceborne Remote Sensing and Digital Image Analysis in Archaeology”, in Siart, C.; Forbriger, M.; Bubenzer, O. (eds.), *Natural Science in Archaeology; Digital Geoarchaeology: New Techniques for Interdisciplinary Human-Environmental Research*, Springer, pp. 109-122

Lasaponara, R. and Masini, N. (2013) “Satellite synthetic aperture radar in archaeology and cultural landscape, an overview”, *Archeol. Prospec*, 20 (2), pp. 71–78.

Lasaponara R. and Masini N. (2012a) “Image Enhancement, Feature Extraction and Geospatial Analysis in an Archaeological Perspective”, in: Lasaponara R., Masini N. (eds), *Satellite Remote Sensing. Remote Sensing and Digital Image Processing*, 16, Springer, pp. 17-63

Lasaponara R. and Masini N. (2012b) “Pattern Recognition and Classification Using VHR Data for Archaeological Research”, in: Lasaponara R., Masini N. (eds), *Satellite Remote Sensing. Remote Sensing and Digital Image Processing*, 16, Springer, pp. 65-85

Lasaponara R. and Masini N. (2012c) “Pan-Sharpening Techniques to Enhance Archaeological Marks: An Overview”, in: Lasaponara R., Masini N. (eds), *Satellite Remote Sensing. Remote Sensing and Digital Image Processing*, vol 16, Springer, pp. 87-109

Lasaponara R. and Masini N. (2012d) “Remote Sensing in Archaeology: From Visual Data Interpretation to Digital Data Manipulation”, in Lasaponara R., Masini N. (eds), *Satellite Remote Sensing. Remote Sensing and Digital Image Processing*, 16, Springer, pp. 65-85

Lasaponara R. and Masini N. (2011), “Satellite Remote Sensing in Archaeology: past, present and future”, *Journal of Archaeological Science*, 38, pp. 1995-2002

Lasaponara, R., and N. Masini. (2007) “Detection of Archaeological Crop Marks by Using Satellite Quickbird Multispectral Imagery”, *Journal of Archaeological Science*, 34, pp. 214–221.

Liew S.C. (2001), Principles of Remote Sensing, CRISP, www.crisp.nus.edu.sg, accessed 15/2/2022

Lillesand M.T., Kiefer W.R. and Chipman W.J. (2015) *Remote sensing and image interpretation*, 7th edition, John Wiley & Sons, New York

Limp W. F. (1993) “Mutlispectral Digital Imagery”, in Jay K. Johnson (ed.), *The Development of Southeastern Archaeology*, The University of Alabama Press, pp. 184-206

Liu, J., Xu, L., Sarris, A. and Topouzi, S. (2003) “CRM & Archaeological Research using Remote Sensing and GIS: Zhouyuan (China) & Lasithi (Greece)”, *CAA Conference 2002 – The digital Heritage of Arhaeology*, pp. 377-384

Luo L., Wang, X., Guo, H., Lasaponara, R., Zong, X., Masini, N., Wang, G., Shi, P., Khatteli, H., Chen, F., Tariq, S., Shao, J., Bachagha, N., Yang, R. and Yao, Y. (2019) “Airborne and spaceborne remote sensing for archaeological and cultural heritage

applications: A review of the century (1907–2017)", *Remote Sensing of Environment*, 232, https://doi.org/10.1016/j.rse.2019.111280

Luo, L., Wang, X., Guo, H., Lasaponara, R., Shi, P., Bachagha, N., Yao, Y., Masini, N., Chen, F., Ji, W., Cao, H., Li, C. and Hu, N. (2018) "Google Earth as a Powerful Tool for Archaeological and Cultural Heritage Applications: A Review", *Remote Sensing*, 10, 1558; doi:10.3390/rs10101558

Luz, L.R., Giongo, V., Santos A.M., Lopes, R., Lima Junior, C. (2022) "Biomass and vegetation index by remote sensing in different caatinga forest areas", *Ciência Rural*, 52.2, http://doi.org/10.1590/0103-8478cr20201104

Masini, N. and Lasaponara, R. (2007) "Investigating the spectral capability of QuickBird data to detect archaeological remains buried under vegetated and not vegetated areas, *J. Cult. Herit.*, 8, pp. 53-60

Matsushita, B., Yang, W., Chen, J., Yuyichi, O. and Guoyu, Q. (2007) "Sensitivity of the Enhanced Vegetation Index (EVI) and Normalized Difference Vegetation Index (NDVI) to Topographic Effects: A Case Study in High-Density Cypress Forest" *Sensors*, 7, pp. 2636 – 2651

Mather, M. P. and Koch M. (2011) *Computer Processing of Remotely-Sensed Images. An Introduction*, 4th edition, Wiley & Sons, UK

Mutanga, O., and Skidmore, A. K. (2004) "Narrow band vegetation indices overcome the saturation problem in biomass estimation", *International journal of remote sensing*, 25(19), pp. 3999-4014.

Morehart, C.T. and Millhauser, J.K. (2016) "Monitoring cultural landscapes from space: Evaluating archaeological sites in the Basin of Mexico using very high-resolution satellite imagery", *Journal of Archaeological Science: Reports*, 10, pp. 363-376

Naji, T. (2018) “Study of vegetation cover distribution using DVI, PVI, WDVI indices with 2D-space plot”, *Journal of Physics: Conference Series*. 1003. 012083. 10.1088/1742-6596/1003/1/012083.

Orlando, P. and Villa, B. (2011), “Remote Sensing applications in archaeology”, *Archaeologia et Calcolatori*, 22, pp. 147-168

Parcak, S. (2017) “Moving from Space-Based to Ground-Based Solutions in Remote Sensing for Archaeological Heritage: A Case Study from Egypt”, *Remote Sensing*, 9(12), 1297

Parcak, S. (2009), *Satellite Remote Sensing for Archaeology*, Routledge, London

Parcak, S. (2007) “Satellite Remote Sensing Methods for Monitoring Archaeological Tells in the Middle East.” *Journal of Field Archaeology*, 32 (1), pp. 65–81.

Pan, Y., Nie, Y., Watene, C., Zhu, J., Liu, F. (2017) “Phenological observations on classical prehistoric sites in the middle and lower reaches of the Yellow River based on Landsat NDVI time series”, *Remote Sens*., 9, 374.

Prabhakara, K. & Hively, W. (2015) “Evaluating the relationship between biomass, percent groundcover and remote sensing indices across six winter cover crop fields in Maryland, United States. International Journal of Applied Earth Observation and Geoinformation”, 39, 10.1016/j.jag.2015.03.002.

Ramzi, A. (2015), “Ground truth mapping capability of urban areas in large scale using GE images”, Proceedings SPIE 9644, Earth Resources and Environmental Remote Sensing / GIS Applications VI, 9644IN (20 October 2015), doi.org/10.1117/12.2193727

Raun, K. H. M., Pfeiffer, M. and Hofle, B. (2018), “Visual Detection and Interpretation of Cultural Remnants on the Königstuhl Hillside in Heidelberg Using Airborne and Terrestrial LiDAR Data”, in Siart, C., Forbriger, M., Bubenzer, O. (eds.), *Natural Science in Archaeology; Digital Geoarchaeology: New Techniques for Interdisciplinary Human-Environmental Research*, Springer, pp. 201-212

Romano, D.G. (2003)," City planning, centuriation and land division in Roman Corinth, *Corinth XX, Corinth the Centenary 1896-1996*, pp. 279-301

Romano, D.G. and Osama, T. (1995) "Remote Sensing, GIS and Electronic Surveying: Reconstructing the City Plan and Landscape of Roman Corinth," in Computer Applications and Quantitative Methods in Archaeology 1994, Jeremy Huggett and Nick Ryan (eds.), *BAR International Series*, 600, pp. 163-174.

Romano, D.G. (1993), "Post-146 B.C. Land Use in Corinth and Planning the Roman Colony of 44 B.C.," in T.E. Gregory (ed.), *The Corinthia in the Roman Period, Journal of Roman Archaeology*, Supplementary Series 8, pp. 9-30

Romano, D.G and Shoenbrun, B.C. (1993) "A computerized architectural and topographical survey of Ancient Corinth", *Journal of Field Archaeology,* 29, pp. 177-90

Ross, S.A., Sobotkova, A. and Burgers, G.J. (2009) "Remote sensing and archaeological prospection in Apulia, Italy", *Journal of Field Archaeology*, 34, pp. 423-437

Rowlands, A. and Sarris, A. (2007) "Detection of exposed and subsurface archaeological remains using multi-sensor remote sensing", *Journal of Archaeological Science*, 34.5, pp. 795-803

Sanders, G.D.R., Palinkas, J., Tzonou-Herbst, I. and Herbst, J. (2018) *Ancient Corinth: Site Guide (7th ed.),* Princeton: ASCSA Publications

Sarp, G. (2014) "Spectral and spatial quality analysis of pan-sharpening algorithms: A case study in Istanbul", *European Journal of Remote Sensing*, 47:1, pp. 19-28

Sarris, A., Papadopoulos, N., Agapiou, A., Salvi, M.C., Hadjimitsis, D., Parkinson, W., Yerkes, R., Gyucha, A. and Duffy, P.R. (2013) "Integration of geophysical surveys, ground hyperspectral measurements, aerial and satellite imagery for archaeological

prospection of prehistoric sites: The case study of Vészto{doubleacute}-Mágor Tell, Hungary", *Journal of Archaeological Science*, 40, pp. 1454–1470

Siart, C., Eitel, B. and Panagiotopoulos, D. (2008) "Investigation of past archaeological landscapes using remote sensing and GIS: a multi-method case study from Mount Ida, Crete", *Journal of Archaeological Science*, 35, pp. 2918-2926

Timothy E. G. (1979), "The Late Roman Wall at Corinth", *Hesperia*, 48 (3), pp. 264-280

Tucker C.J. (1979) "Red and photographic infrared linear combinations for monitoring vegetation", *Remote Sensing of Environment*, 8, pp. 127-150

Upadhyay R.K., Kishore N. and Sharma M. (2021) "Delineation and mapping of palaeochannels using remote sensing, geophysical, and sedimentological techniques: A comprehensive approach", *Water Science*, 35:1, pp. 100-108

Zanni, S. and De Rosa, A. (2019) "Remote Sensing Analyses on Sentinel-2 Images: Looking for Roman Roads in Srem Region (Serbia)", Geosciences 9, 1: 25, https://doi.org/10.3390/geosciences9010025

APPENDICES

Appendix I

Error matrix for vegetation indices unsupervised classification. General study area.

DVI					
Class	**Anomalies**	**Vegetation**	**Total**		
Anomalies	67	330	397		Overall accuracy 16.88%
Vegetation	0	0	0		
Total	67	330	397		
EVI					
Class	**Anomalies**	**Vegetation**	**Total**		
Anomalies	41	356	397		Overall accuracy 10.33%
Vegetation	0	0	0		
Total	41	356	397		
NDVI					
Class	**Anomalies**	**Vegetation**	**Total**		
Anomalies	163	234	397		Overall accuracy 41.06%
Vegetation	0	0	0		
Total	163	234	397		
SAVI					
Class	**Anomalies**	**Vegetation**	**Total**		
Anomalies	146	251	397		Overall accuracy 36.78%
Vegetation	0	0	0		
Total	146	251	397		
SQRT/SR					
Class	**Anomalies**	**Vegetation**	**Total**		
Anomalies	148	249	397		Overall accuarcy 37.28%
Vegetation	0	0	0		
Total	148	249	397		
SR					
Class	**Anomalies**	**Vegetation**	**Total**		
Anomalies	148	249	397		Overall accuarcy 37.28%
Vegetation	0	0	0		
Total	148	249	397		
MSR					
Class	**Anomalies**	**Vegetation**	**Total**		
Anomalies	28	369	397		Overall accuracy 7.05%
Vegetation	0	0	0		
Total	28	369	397		
MSAVI					
Class	**Anomalies**	**Vegetation**	**Total**		
Anomalies	152	245	397		Overall accuracy 38.29%
Vegetation	0	0	0		
Total	152	245	397		

Appendix II

Error matrix for vegetation indices unsupervised classification. West of soccer field area.

DVI					
Class	**Anomalies**	**Vegetation**	**Total**		
Anomalies	5	58	63		Overall accuracy 7.94%
Vegetation	0	0	0		
Total	5	58	63		
EVI					
Class	**Anomalies**	**Vegetation**	**Total**		
Anomalies	15	48	63		Overall accuracy 23.81%
Vegetation	0	0	0		
Total	15	48	63		
NDVI					
Class	**Anomalies**	**Vegetation**	**Total**		
Anomalies	8	55	63		Overall accuracy 12.7%
Vegetation	0	0	0		
Total	8	55	63		
SAVI					
Class	**Anomalies**	**Vegetation**	**Total**		
Anomalies	8	55	63		Overall accuracy 12.7%
Vegetation	0	0	0		
Total	8	55	63		
SQRT/SR					
Class	**Anomalies**	**Vegetation**	**Total**		
Anomalies	8	55	63		Overall accuracy 12.7%
Vegetation	0	0	0		
Total	8	55	63		
SR					
Class	**Anomalies**	**Vegetation**	**Total**		
Anomalies	8	55	63		Overall accuracy 12.7%
Vegetation	0	0	0		
Total	8	55	63		
MSR					
Class	**Anomalies**	**Vegetation**	**Total**		
Anomalies	5	58	63		Overall accuracy 7.94%
Vegetation	0	0	0		
Total	5	58	63		
MSAVI					
Class	**Anomalies**	**Vegetation**	**Total**		
Anomalies	8	55	63		Overall accuracy 12.7%
Vegetation	0	0	0		
Total	8	55	63		

Appendix III

Error matrix for vegetation indices unsupervised classification. Late Roman wall area.

DVI					
Class	**Anomalies**	**Vegetation**	**Total**		
Anomalies	14	39	53		Overall accuracy 26.42%
Vegetation	0	0	0		
Total	14	39	53		
EVI					
Class	**Anomalies**	**Vegetation**	**Total**		
Anomalies	8	45	53		Overall accuracy 15.09%
Vegetation	0	0	0		
Total	8	45	53		
NDVI					
Class	**Anomalies**	**Vegetation**	**Total**		
Anomalies	25	28	53		Overall accuarcy 47.17%
Vegetation	0	0	0		
Total	25	28	53		
SAVI					
Class	**Anomalies**	**Vegetation**	**Total**		
Anomalies	23	30	53		Overall accuracy 43.4%
Vegetation	0	0	0		
Total	23	30	53		
SQRT/SR					
Class	**Anomalies**	**Vegetation**	**Total**		
Anomalies	24	29	53		Overall accuracy 45.28%
Vegetation	0	0	0		
Total	24	29	53		
SR					
Class	**Anomalies**	**Vegetation**	**Total**		
Anomalies	24	29	53		Overall accuracy 45.28%
Vegetation	0	0	0		
Total	24	29	53		
MSR					
Class	**Anomalies**	**Vegetation**	**Total**		
Anomalies	8	45	53		Overall accuracy 15.09%
Vegetation	0	0	0		
Total	8	45	53		
MSAVI					
Class	**Anomalies**	**Vegetation**	**Total**		
Anomalies	25	28	53		Overall accuracy 47.17%
Vegetation	0	0	0		
Total	25	28	53		

Appendix IV

Error matrix for supervised classification of study area.

Composite Image						
Class	**Vegetation**	**Soil/Sparse vegetation**	**Tile roofs**	**Roads/Impervious**	**Archaeology/Rocks**	**Total**
Vegetation	50	0	0	0	0	50
Soil/Sparse vegetation	0	41	2	0	7	50
Tile roofs	0	1	49	0	0	50
Roads/Impervious	0	0	0	42	8	50
Archaeology/Rocks	1	0	0	0	49	50
Total	51	42	51	42	64	250
Overall accuracy 92.4% κ =0.9						
Vegetation: User Accuracy 100% / Producer Accuracy 98.04%						
Soil/Sparse vegetation: User accuracy 82% / Producer accuracy 97.62%						
Tile roofs: User accuracy 98% / Producer accuracy 96.08%						
Roads/Impervious: User accuracy 84% / Producer accuracy 100%						
Archaeology/Rocks: User accuracy 98% Producer accuracy 76.56%						
Blue band						
Class	**Vegetation**	**Soil/Sparse vegetation**	**Tile roofs**	**Roads/Impervious**	**Archaeology/Rocks**	**Total**
Vegetation	48	2	0	0	0	50
Soil/Sparse vegetation	1	20	23	0	6	50
Tile roofs	3	13	26	0	8	50
Roads/Impervious	0	0	0	22	28	50
Archaeology/Rocks	0	2	13	4	31	50
Total	52	37	62	26	73	250
Overall accuracy 58.8% κ =0.49						
Vegetation: User Accuracy 96% / Producer Accuracy 92.31%						
Soil/Sparse vegetation: User accuracy 40% / Producer accuracy 54.05%						
Tile roofs: User accuracy 52% / Producer accuracy 41.94%						
Roads/Impervious: User accuracy 44% / Producer accuracy 84.62%						
Archaeology/Rocks: User accuracy 62% Producer accuracy 42.47%						
Red band						
Class	**Vegetation**	**Soil/Sparse vegetation**	**Tile roofs**	**Roads/Impervious**	**Archaeology/Rocks**	**Total**
Vegetation	50	0	0	0	0	50
Soil/Sparse vegetation	0	34	5	3	8	50
Tile roofs	0	5	39	3	3	50
Roads/Impervious	0	5	26	4	15	50
Archaeology/Rocks	0	25	13	1	11	50
Total	50	69	83	11	37	250
Overall accuracy 55.2% κ =0.44						
Vegetation: User Accuracy 100% / Producer Accuracy 100%						
Soil/Sparse vegetation: User accuracy 68% / Producer accuracy 49.28%						
Tile roofs: User accuracy 78% / Producer accuracy 46.99%						
Roads/Impervious: User accuracy 8% / Producer accuracy 36.36%						
Archaeology/Rocks: User accuracy 22% Producer accuracy 29.73%						

NIR band						
Class	**Vegetation**	**Soil/Sparse vegetation**	**Tile roofs**	**Roads/Impervious**	**Archaeology/Rocks**	**Total**
Vegetation	33	2	6	0	9	50
Soil/Sparse vegetation	1	28	3	3	15	50
Tile roofs	15	5	13	2	15	50
Roads/Impervious	10	12	9	4	15	50
Archaeology/Rocks	6	17	8	0	19	50
Total	65	64	39	9	73	250

Overall accuracy 38.8% κ =0.23

Vegetation: User Accuracy 66% / Producer Accuracy 50.77%

Soil/Sparse vegetation: User accuracy 56% / Producer accuracy 43.75%

Tile roofs: User accuracy 26% / Producer accuracy 33.33%

Roads/Impervious: User accuracy 8% / Producer accuracy 44.44%

Archaeology/Rocks: User accuracy 38% Producer accuracy 26.03%

NDVI						
Class	**Vegetation**	**Soil/Sparse vegetation**	**Tile roofs**	**Roads/Impervious**	**Archaeology/Rocks**	**Total**
Vegetation	50	0	0	0	0	50
Soil/Sparse vegetation	0	10	15	4	21	50
Tile roofs	0	0	43	3	4	50
Roads/Impervious	0	0	45	4	1	50
Archaeology/Rocks	0	7	19	7	17	50
Total	50	17	122	18	43	250

Overall accuracy 49.6% κ =0.37

Vegetation: User Accuracy 100% / Producer Accuracy 100%

Soil/Sparse vegetation: User accuracy 20% / Producer accuracy 58.82%

Tile roofs: User accuracy 86% / Producer accuracy 35.25%

Roads/Impervious: User accuracy 8% / Producer accuracy 22.22%

Archaeology/Rocks: User accuracy 34% Producer accuracy 39.53%

Appendix V

Error matrix for unsupervised classification of study area.

Composite image						
Class	**Vegetation**	**Soil/Sparse vegetation**	**Tile roofs**	**Roads/Impervious**	**Archaeology/Rocks**	**Total**
Vegetation	50	0	0	0	0	50
Soil/Sparse vegetation	0	8	0	4	38	50
Tile roofs	0	1	0	42	7	50
Roads/Impervious	0	0	0	46	4	50
Archaeology/Rocks	1	1	0	16	32	50
Total	51	10	0	108	81	250
Overall accuracy 54.4% κ=0.43						
Vegetation: User Accuracy 100% / Producer Accuracy 98.04%						
Soil/Sparse vegetation: User accuracy 16% / Producer accuracy 80%						
Tile roofs: User accuracy 0 / Producer accuracy 0						
Roads/Impervious: User accuracy 92% / Producer accuracy 42.59%						
Archaeology/Rocks: User accuracy 64% Producer accuracy 39.51%						
Blue band						
Class	**Vegetation**	**Soil/Sparse vegetation**	**Tile roofs**	**Roads/Impervious**	**Archaeology/Rocks**	**Total**
Vegetation	50	0	0	0	0	50
Soil/Sparse vegetation	6	18	0	3	23	50
Tile roofs	4	16	0	3	27	50
Roads/Impervious	0	0	0	49	1	50
Archaeology/Rocks	0	2	0	26	22	50
Total	60	36	0	81	73	250
Overall accuracy 55.6% κ =0.45						
Vegetation: User Accuracy 100% / Producer Accuracy 83.33%						
Soil/Sparse vegetation: User accuracy 36% / Producer accuracy 50%						
Tile roofs: User accuracy 0 / Producer accuracy 0						
Roads/Impervious: User accuracy 98% / Producer accuracy 60.49%						
Archaeology/Rocks: User accuracy 44% Producer accuracy 30.14%						
Red band						
Class	**Vegetation**	**Soil/Sparse vegetation**	**Tile roofs**	**Roads/Impervious**	**Archaeology/Rocks**	**Total**
Vegetation	50	0	0	0	0	50
Soil/Sparse vegetation	1	8	0	28	13	50
Tile roofs	0	2	0	29	19	50
Roads/Impervious	0	0	0	24	26	50
Archaeology/Rocks	0	5	0	24	21	50
Total	51	15	0	105	79	250
Overall accuracy 41.2% κ =0.27						
Vegetation: User Accuracy 100% / Producer Accuracy 98.04%						
Soil/Sparse vegetation: User accuracy 16% / Producer accuracy 53.33%						
Tile roofs: User accuracy 0 / Producer accuracy 0						
Roads/Impervious: User accuracy 48% / Producer accuracy 22.86%						
Archaeology/Rocks: User accuracy 42% Producer accuracy 26.58%						

NIR band						
Class	**Vegetation**	**Soil/Sparse vegetation**	**Tile roofs**	**Roads/Impervious**	**Archaeology/Rocks**	**Total**
Vegetation	50	0	0	0	0	50
Soil/Sparse vegetation	0	20	0	29	1	50
Tile roofs	0	3	0	47	0	50
Roads/Impervious	0	0	0	50	0	50
Archaeology/Rocks	0	17	0	27	6	50
Total	50	40	0	153	7	250

Overall accuracy 50.4% κ =0.38

Vegetation: User Accuracy 100% / Producer Accuracy 100%

Soil/Sparse vegetation: User accuracy 40% / Producer accuracy 50%

Tile roofs: User accuracy 0 / Producer accuracy 0

Roads/Impervious: User accuracy 100% / Producer accuracy 32.68%

Archaeology/Rocks: User accuracy 12% Producer accuracy 85.71%

NDVI						
Class	**Vegetation**	**Soil/Sparse vegetation**	**Tile roofs**	**Roads/Impervious**	**Archaeology/Rocks**	**Total**
Vegetation	35	6	0	0	9	50
Soil/Sparse vegetation	3	16	0	26	5	50
Tile roofs	18	6	0	4	22	50
Roads/Impervious	14	13	0	10	13	50
Archaeology/Rocks	7	16	0	10	17	50
Total	77	57	0	50	66	250

Overall accuracy 31.2% κ =0.14

Vegetation: User Accuracy 70% / Producer Accuracy 46.45%

Soil/Sparse vegetation: User accuracy 32% / Producer accuracy 28.07%

Tile roofs: User accuracy 0 / Producer accuracy 0

Roads/Impervious: User accuracy 20% / Producer accuracy 20%

Archaeology/Rocks: User accuracy 34% Producer accuracy 25.76%

Series from Lund University

Department of Physical Geography and Ecosystem Science

Master Thesis in Geographical Information Science

1. *Anthony Lawther:* The application of GIS-based binary logistic regression for slope failure susceptibility mapping in the Western Grampian Mountains, Scotland (2008).
2. *Rickard Hansen:* Daily mobility in Grenoble Metropolitan Region, France. Applied GIS methods in time geographical research (2008).
3. *Emil Bayramov:* Environmental monitoring of bio-restoration activities using GIS and Remote Sensing (2009).
4. *Rafael Villarreal Pacheco:* Applications of Geographic Information Systems as an analytical and visualization tool for mass real estate valuation: a case study of Fontibon District, Bogota, Columbia (2009).
5. *Siri Oestreich Waage:* a case study of route solving for oversized transport: The use of GIS functionalities in transport of transformers, as part of maintaining a reliable power infrastructure (2010).
6. *Edgar Pimiento:* Shallow landslide susceptibility – Modelling and validation (2010).
7. *Martina Schäfer:* Near real-time mapping of floodwater mosquito breeding sites using aerial photographs (2010).
8. *August Pieter van Waarden-Nagel:* Land use evaluation to assess the outcome of the programme of rehabilitation measures for the river Rhine in the Netherlands (2010).
9. *Samira Muhammad:* Development and implementation of air quality data mart for Ontario, Canada: A case study of air quality in Ontario using OLAP tool. (2010).
10. *Fredros Oketch Okumu*: Using remotely sensed data to explore spatial and temporal relationships between photosynthetic productivity of vegetation and malaria transmission intensities in selected parts of Africa (2011).
11. *Svajunas Plunge:* Advanced decision support methods for solving diffuse water pollution problems (2011).
12. *Jonathan Higgins:* Monitoring urban growth in greater Lagos: A case study using GIS to monitor the urban growth of Lagos 1990 - 2008 and produce future growth prospects for the city (2011).
13. *Mårten Karlberg:* Mobile Map Client API: Design and Implementation for Android (2011).
14. *Jeanette McBride:* Mapping Chicago area urban tree canopy using color infrared imagery (2011).

15. *Andrew Farina:* Exploring the relationship between land surface temperature and vegetation abundance for urban heat island mitigation in Seville, Spain (2011).

16. *David Kanyari*: Nairobi City Journey Planner: An online and a Mobile Application (2011).

17. *Laura V. Drews:* Multi-criteria GIS analysis for siting of small wind power plants - A case study from Berlin (2012).

18. *Qaisar Nadeem:* Best living neighborhood in the city - A GIS based multi criteria evaluation of ArRiyadh City (2012).

19. *Ahmed Mohamed El Saeid Mustafa:* Development of a photo voltaic building rooftop integration analysis tool for GIS for Dokki District, Cairo, Egypt (2012).

20. *Daniel Patrick Taylor*: Eastern Oyster Aquaculture: Estuarine Remediation via Site Suitability and Spatially Explicit Carrying Capacity Modeling in Virginia's Chesapeake Bay (2013).

21. *Angeleta Oveta Wilson:* A Participatory GIS approach to *unearthing* Manchester's Cultural Heritage '*gold mine'* (2013).

22. *Ola Svensson:* Visibility and Tholos Tombs in the Messenian Landscape: A Comparative Case Study of the Pylian Hinterlands and the Soulima Valley (2013).

23. *Monika Ogden:* Land use impact on water quality in two river systems in South Africa (2013).

24. *Stefan Rova:* A GIS based approach assessing phosphorus load impact on Lake Flaten in Salem, Sweden (2013).

25. *Yann Buhot:* Analysis of the history of landscape changes over a period of 200 years. How can we predict past landscape pattern scenario and the impact on habitat diversity? (2013).

26. *Christina Fotiou:* Evaluating habitat suitability and spectral heterogeneity models to predict weed species presence (2014).

27. *Inese Linuza:* Accuracy Assessment in Glacier Change Analysis (2014).

28. *Agnieszka Griffin:* Domestic energy consumption and social living standards: a GIS analysis within the Greater London Authority area (2014).

29. *Brynja Guðmundsdóttir:* Detection of potential arable land with remote sensing and GIS - A Case Study for Kjósarhreppur (2014).

30. *Oleksandr Nekrasov:* Processing of MODIS Vegetation Indices for analysis of agricultural droughts in the southern Ukraine between the years 2000-2012 (2014).

31. *Sarah Tressel:* Recommendations for a polar Earth science portal in the context of Arctic Spatial Data Infrastructure (2014).

32. *Caroline Gevaert:* Combining Hyperspectral UAV and Multispectral Formosat-2 Imagery for Precision Agriculture Applications (2014).

33. *Salem Jamal-Uddeen:* Using GeoTools to implement the multi-criteria evaluation analysis - weighted linear combination model (2014).

34. *Samanah Seyedi-Shandiz:* Schematic representation of geographical railway network at the Swedish Transport Administration (2014).

35. *Kazi Masel Ullah:* Urban Land-use planning using Geographical Information System and analytical hierarchy process: case study Dhaka City (2014).

36. *Alexia Chang-Wailing Spitteler:* Development of a web application based on MCDA and GIS for the decision support of river and floodplain rehabilitation projects (2014).

37. *Alessandro De Martino:* Geographic accessibility analysis and evaluation of potential changes to the public transportation system in the City of Milan (2014).

38. *Alireza Mollasalehi:* GIS Based Modelling for Fuel Reduction Using Controlled Burn in Australia. Case Study: Logan City, QLD (2015).

39. *Negin A. Sanati:* Chronic Kidney Disease Mortality in Costa Rica; Geographical Distribution, Spatial Analysis and Non-traditional Risk Factors (2015).

40. *Karen McIntyre:* Benthic mapping of the Bluefields Bay fish sanctuary, Jamaica (2015).

41. *Kees van Duijvendijk:* Feasibility of a low-cost weather sensor network for agricultural purposes: A preliminary assessment (2015).

42. *Sebastian Andersson Hylander:* Evaluation of cultural ecosystem services using GIS (2015).

43. *Deborah Bowyer:* Measuring Urban Growth, Urban Form and Accessibility as Indicators of Urban Sprawl in Hamilton, New Zealand (2015).

44. *Stefan Arvidsson:* Relationship between tree species composition and phenology extracted from satellite data in Swedish forests (2015).

45. *Damián Giménez Cruz*: GIS-based optimal localisation of beekeeping in rural Kenya (2016).

46. *Alejandra Narváez Vallejo:* Can the introduction of the topographic indices in LPJ-GUESS improve the spatial representation of environmental variables? (2016).

47. *Anna Lundgren:* Development of a method for mapping the highest coastline in Sweden using breaklines extracted from high resolution digital elevation models (2016).

48. *Oluwatomi Esther Adejoro:* Does location also matter? A spatial analysis of social achievements of young South Australians (2016).

49. *Hristo Dobrev Tomov:* Automated temporal NDVI analysis over the Middle East for the period 1982 - 2010 (2016).

50. *Vincent Muller:* Impact of Security Context on Mobile Clinic Activities A GIS Multi Criteria Evaluation based on an MSF Humanitarian Mission in Cameroon (2016).

51. *Gezahagn Negash Seboka:* Spatial Assessment of NDVI as an Indicator of Desertification in Ethiopia using Remote Sensing and GIS (2016).

52. *Holly Buhler:* Evaluation of Interfacility Medical Transport Journey Times in Southeastern British Columbia. (2016).

53. *Lars Ole Grottenberg*: Assessing the ability to share spatial data between emergency management organisations in the High North (2016).

54. *Sean Grant:* The Right Tree in the Right Place: Using GIS to Maximize the Net Benefits from Urban Forests (2016).

55. *Irshad Jamal:* Multi-Criteria GIS Analysis for School Site Selection in Gorno-Badakhshan Autonomous Oblast, Tajikistan (2016).

56. *Fulgencio Sanmartín:* Wisdom-volkano: A novel tool based on open GIS and time-series visualization to analyse and share volcanic data (2016).

57. *Nezha Acil:* Remote sensing-based monitoring of snow cover dynamics and its influence on vegetation growth in the Middle Atlas Mountains (2016).

58. *Julia Hjalmarsson:* A Weighty Issue: Estimation of Fire Size with Geographically Weighted Logistic Regression (2016).

59. *Mathewos Tamiru Amato:* Using multi-criteria evaluation and GIS for chronic food and nutrition insecurity indicators analysis in Ethiopia (2016).

60. *Karim Alaa El Din Mohamed Soliman El Attar:* Bicycling Suitability in Downtown, Cairo, Egypt (2016).

61. *Gilbert Akol Echelai:* Asset Management: Integrating GIS as a Decision Support Tool in Meter Management in National Water and Sewerage Corporation (2016).

62. *Terje Slinning:* Analytic comparison of multibeam echo soundings (2016).

63. *Gréta Hlín Sveinsdóttir:* GIS-based MCDA for decision support: A framework for wind farm siting in Iceland (2017).

64. *Jonas Sjögren:* Consequences of a flood in Kristianstad, Sweden: A GIS-based analysis of impacts on important societal functions (2017).

65. *Nadine Raska:* 3D geologic subsurface modelling within the Mackenzie Plain, Northwest Territories, Canada (2017).

66. *Panagiotis Symeonidis*: Study of spatial and temporal variation of atmospheric optical parameters and their relation with PM 2.5 concentration over Europe using GIS technologies (2017).

67. *Michaela Bobeck:* A GIS-based Multi-Criteria Decision Analysis of Wind Farm Site Suitability in New South Wales, Australia, from a Sustainable Development Perspective (2017).

68. *Raghdaa Eissa*: Developing a GIS Model for the Assessment of Outdoor Recreational Facilities in New Cities Case Study: Tenth of Ramadan City, Egypt (2017).

69. *Zahra Khais Shahid*: Biofuel plantations and isoprene emissions in Svea and Götaland (2017).

70. *Mirza Amir Liaquat Baig*: Using geographical information systems in epidemiology: Mapping and analyzing occurrence of diarrhea in urban - residential area of Islamabad, Pakistan (2017).

71. *Joakim Jörwall*: Quantitative model of Present and Future well-being in the EU-28: A spatial Multi-Criteria Evaluation of socioeconomic and climatic comfort factors (2017).

72. *Elin Haettner*: Energy Poverty in the Dublin Region: Modelling Geographies of Risk (2017).

73. *Harry Eriksson*: Geochemistry of stream plants and its statistical relations to soil- and bedrock geology, slope directions and till geochemistry. A GIS-analysis of small catchments in northern Sweden (2017).

74. *Daniel Gardevärn:* PPGIS and Public meetings – An evaluation of public participation methods for urban planning (2017).

75. *Kim Friberg:* Sensitivity Analysis and Calibration of Multi Energy Balance Land Surface Model Parameters (2017).

76. *Viktor Svanerud:* Taking the bus to the park? A study of accessibility to green areas in Gothenburg through different modes of transport (2017).

77. *Lisa-Gaye Greene*: Deadly Designs: The Impact of Road Design on Road Crash Patterns along Jamaica's North Coast Highway (2017).

78. *Katarina Jemec Parker*: Spatial and temporal analysis of fecal indicator bacteria concentrations in beach water in San Diego, California (2017).

79. *Angela Kabiru*: An Exploratory Study of Middle Stone Age and Later Stone Age Site Locations in Kenya's Central Rift Valley Using Landscape Analysis: A GIS Approach (2017).

80. *Kristean Björkmann*: Subjective Well-Being and Environment: A GIS-Based Analysis (2018).

81. *Williams Erhunmonmen Ojo*: Measuring spatial accessibility to healthcare for people living with HIV-AIDS in southern Nigeria (2018).

82. *Daniel Assefa*: Developing Data Extraction and Dynamic Data Visualization (Styling) Modules for Web GIS Risk Assessment System (WGRAS). (2018).

83. *Adela Nistora*: Inundation scenarios in a changing climate: assessing potential impacts of sea-level rise on the coast of South-East England (2018).

84. *Marc Seliger*: Thirsty landscapes - Investigating growing irrigation water consumption and potential conservation measures within Utah's largest master-planned community: Daybreak (2018).

85. *Luka Jovičić*: Spatial Data Harmonisation in Regional Context in Accordance with INSPIRE Implementing Rules (2018).

86. *Christina Kourdounouli*: Analysis of Urban Ecosystem Condition Indicators for the Large Urban Zones and City Cores in EU (2018).

87. *Jeremy Azzopardi*: Effect of distance measures and feature representations on distance-based accessibility measures (2018).

88. *Patrick Kabatha*: An open source web GIS tool for analysis and visualization of elephant GPS telemetry data, alongside environmental and anthropogenic variables (2018).

89. *Richard Alphonce Giliba*: Effects of Climate Change on Potential Geographical Distribution of Prunus africana (African cherry) in the Eastern Arc Mountain Forests of Tanzania (2018).

90. *Eiður Kristinn Eiðsson*: Transformation and linking of authoritative multi-scale geodata for the Semantic Web: A case study of Swedish national building data sets (2018).

91. *Niamh Harty*: HOP!: a PGIS and citizen science approach to monitoring the condition of upland paths (2018).

92. *José Estuardo Jara Alvear*: Solar photovoltaic potential to complement hydropower in Ecuador: A GIS-based framework of analysis (2018).

93. *Brendan O'Neill*: Multicriteria Site Suitability for Algal Biofuel Production Facilities (2018).

94. *Roman Spataru*: Spatial-temporal GIS analysis in public health – a case study of polio disease (2018).

95. *Alicja Miodońska*: Assessing evolution of ice caps in Suðurland, Iceland, in years 1986 - 2014, using multispectral satellite imagery (2019).

96. *Dennis Lindell Schettini*: A Spatial Analysis of Homicide Crime's Distribution and Association with Deprivation in Stockholm Between 2010-2017 (2019).

97. *Damiano Vesentini*: The Po Delta Biosphere Reserve: Management challenges and priorities deriving from anthropogenic pressure and sea level rise (2019).

98. *Emilie Arnesten*: Impacts of future sea level rise and high water on roads, railways and environmental objects: a GIS analysis of the potential effects of increasing sea levels and highest projected high water in Scania, Sweden (2019).

99. *Syed Muhammad Amir Raza*: Comparison of geospatial support in RDF stores: Evaluation for ICOS Carbon Portal metadata (2019).

100. *Hemin Tofiq*: Investigating the accuracy of Digital Elevation Models from UAV images in areas with low contrast: A sandy beach as a case study (2019).

101. *Evangelos Vafeiadis*: Exploring the distribution of accessibility by public transport using spatial analysis. A case study for retail concentrations and public hospitals in Athens (2019).

102. *Milan Sekulic*: Multi-Criteria GIS modelling for optimal alignment of roadway by-passes in the Tlokweng Planning Area, Botswana (2019).

103. *Ingrid Piirisaar*: A multi-criteria GIS analysis for siting of utility-scale photovoltaic solar plants in county Kilkenny, Ireland (2019).

104. *Nigel Fox*: Plant phenology and climate change: possible effect on the onset of various wild plant species' first flowering day in the UK (2019).

105. *Gunnar Hesch*: Linking conflict events and cropland development in Afghanistan, 2001 to 2011, using MODIS land cover data and Uppsala Conflict Data Programme (2019).

106. *Elijah Njoku*: Analysis of spatial-temporal pattern of Land Surface Temperature (LST) due to NDVI and elevation in Ilorin, Nigeria (2019).

107. *Katalin Bunyevácz*: Development of a GIS methodology to evaluate informal urban green areas for inclusion in a community governance program (2019).

108. *Paul dos Santos*: Automating synthetic trip data generation for an agent-based simulation of urban mobility (2019).

109. *Robert O' Dwyer*: Land cover changes in Southern Sweden from the mid-Holocene to present day: Insights for ecosystem service assessments (2019).

110. *Daniel Klingmyr*: Global scale patterns and trends in tropospheric NO2 concentrations (2019).

111. *Marwa Farouk Elkabbany*: Sea Level Rise Vulnerability Assessment for Abu Dhabi, United Arab Emirates (2019).

112. *Jip Jan van Zoonen*: Aspects of Error Quantification and Evaluation in Digital Elevation Models for Glacier Surfaces (2020).

113. *Georgios Efthymiou*: The use of bicycles in a mid-sized city – benefits and obstacles identified using a questionnaire and GIS (2020).

114. *Haruna Olayiwola Jimoh*: Assessment of Urban Sprawl in MOWE/IBAFO Axis of Ogun State using GIS Capabilities (2020).

115. *Nikolaos Barmpas Zachariadis*: Development of an iOS, Augmented Reality for disaster management (2020).

116. *Ida Storm*: ICOS Atmospheric Stations: Spatial Characterization of CO2 Footprint Areas and Evaluating the Uncertainties of Modelled CO2 Concentrations (2020).

117. *Alon Zuta*: Evaluation of water stress mapping methods in vineyards using airborne thermal imaging (2020).

118. *Marcus Eriksson*: Evaluating structural landscape development in the municipality Upplands-Bro, using landscape metrics indices (2020).

119. *Ane Rahbek Vierø*: Connectivity for Cyclists? A Network Analysis of Copenhagen's Bike Lanes (2020).

120. *Cecilia Baggini*: Changes in habitat suitability for three declining Anatidae species in saltmarshes on the Mersey estuary, North-West England (2020).

121. *Bakrad Balabanian*: Transportation and Its Effect on Student Performance (2020).

122. *Ali Al Farid*: Knowledge and Data Driven Approaches for Hydrocarbon Microseepage Characterizations: An Application of Satellite Remote Sensing (2020).

123. *Bartlomiej Kolodziejczyk*: Distribution Modelling of Gene Drive-Modified Mosquitoes and Their Effects on Wild Populations (2020).

124. *Alexis Cazorla*: Decreasing organic nitrogen concentrations in European water bodies - links to organic carbon trends and land cover (2020).

125. *Kharid Mwakoba*: Remote sensing analysis of land cover/use conditions of community-based wildlife conservation areas in Tanzania (2021).

126. *Chinatsu Endo*: Remote Sensing Based Pre-Season Yellow Rust Early Warning in Oromia, Ethiopia (2021).

127. *Berit Mohr*: Using remote sensing and land abandonment as a proxy for long-term human out-migration. A Case Study: Al-Hassakeh Governorate, Syria (2021).

128. *Kanchana Nirmali Bandaranayake*: Considering future precipitation in delineation locations for water storage systems - Case study Sri Lanka (2021).

129. *Emma Bylund*: Dynamics of net primary production and food availability in the aftermath of the 2004 and 2007 desert locust outbreaks in Niger and Yemen (2021).

130. *Shawn Pace*: Urban infrastructure inundation risk from permanent sea-level rise scenarios in London (UK), Bangkok (Thailand) and Mumbai (India): A comparative analysis (2021).

131. *Oskar Evert Johansson*: The hydrodynamic impacts of Estuarine Oyster reefs, and the application of drone technology to this study (2021).

132. *Pritam Kumarsingh*: A Case Study to develop and test GIS/SDSS methods to assess the production capacity of a Cocoa Site in Trinidad and Tobago (2021).

133. *Muhammad Imran Khan*: Property Tax Mapping and Assessment using GIS (2021).

134. *Domna Kanari*: Mining geosocial data from Flickr to explore tourism patterns: The case study of Athens (2021).

135. *Mona Tykesson Klubien*: Livestock-MRSA in Danish pig farms (2021).

136. *Ove Njøten*: Comparing radar satellites. Use of Sentinel-1 leads to an increase in oil spill alerts in Norwegian waters (2021).

137. *Panagiotis Patrinos*: Change of heating fuel consumption patterns produced by the economic crisis in Greece (2021).

138. *Lukasz Langowski*: Assessing the suitability of using Sentinel-1A SAR multi-temporal imagery to detect fallow periods between rice crops (2021).

139. *Jonas Tillman*: Perception accuracy and user acceptance of legend designs for opacity data mapping in GIS (2022).

140. *Gabriela Olekszyk*: ALS (Airborne LIDAR) accuracy: Can potential low data quality of ground points be modelled/detected? Case study of 2016 LIDAR capture over Auckland, New Zealand (2022).

141. *Luke Aspland*: Weights of Evidence Predictive Modelling in Archaeology (2022).

142. *Luís Fareleira Gomes*: The influence of climate, population density, tree species and land cover on fire pattern in mainland Portugal (2022).

143. *Andreas Eriksson*: Mapping Fire Salamander (Salamandra salamandra) Habitat Suitability in Baden-Württemberg with Multi-Temporal Sentinel-1 and Sentinel-2 Imagery (2022).

144. *Lisbet Hougaard Baklid*: Geographical expansion rate of a brown bear population in Fennoscandia and the factors explaining the directional variations (2022).

145. *Victoria Persson*: Mussels in deep water with climate change: Spatial distribution of mussel (Mytilus galloprovincialis) growth offshore in the French Mediterranean with respect to climate change scenario RCP 8.5 Long Term and Integrated Multi-Trophic Aquaculture (IMTA) using Dynamic Energy Budget (DEB) modelling (2022).

146. *Benjamin Bernard Fabien Gérard Borgeais*: Implementing a multi-criteria GIS analysis and predictive modelling to locate Upper Palaeolithic decorated caves in the Périgord noir, France (2022).

147. *Bernat Dorado-Guerrero*: Assessing the impact of post-fire restoration interventions using spectral vegetation indices: A case study in El Bruc, Spain (2022).

148. *Ignatius Gabriel Aloysius Maria Perera*: The Influence of Natural Radon Occurrence on the Severity of the COVID-19 Pandemic in Germany: A Spatial Analysis (2022).

149. *Mark Overton*: An Analysis of Spatially-enabled Mobile Decision Support Systems in a Collaborative Decision-Making Environment (2022).

150. *Viggo Lunde*: Analysing methods for visualizing time-series datasets in open-source web mapping (2022).

151. *Johan Viscarra Hansson*: Distribution Analysis of Impatiens glandulifera in Kronoberg County and a Pest Risk Map for Alvesta Municipality (2022).

152. *Vincenzo Poppiti*: GIS and Tourism: Developing strategies for new touristic flows after the Covid-19 pandemic (2022).

153. *Henrik Hagelin*: Wildfire growth modelling in Sweden - A suitability assessment of available data (2023).

154. *Gabriel Romeo Ferriols Pavico*: Where there is road, there is fire (influence): An exploratory study on the influence of roads in the spatial patterns of Swedish wildfires of 2018 (2023).

155. *Colin Robert Potter*: Using a GIS to enable an economic, land use and energy output comparison between small wind powered turbines and large-scale wind farms: the case of Oslo, Norway (2023).

156. *Krystyna Muszel*: Impact of Sea Surface Temperature and Salinity on Phytoplankton blooms phenology in the North Sea (2023).

157. *Tobias Rydlinge*: Urban tree canopy mapping - an open source deep learning approach (2023).

158. *Albert Wellendorf*: Multi-scale Bark Beetle Predictions Using Machine Learning (2023).

159. *Manolis Papadakis*: Use of Satellite Remote Sensing for Detecting Archaeological Features: An Example from Ancient Corinth, Greece (2023).